Master of Science Thesis in Electrical Engineering
Department of Electrical Engineering, Linköping University, 2017

Compressible Flow Modeling with Combustion Engine Applications

Carl Vilhelmsson

LINKÖPING
UNIVERSITY

Master of Science Thesis in Electrical Engineering

Compressible Flow Modeling with Combustion Engine Applications

Carl Vilhelmsson

LiTH-ISY-EX--17/5055--SE

Supervisor: **Robin Holmbom**
ISY, Linköpings University
Samuel Alfredsson
Volvo Car Corporation
Marcus Rubensson
Volvo Car Corporation

Examiner: **Professor Lars Eriksson**
ISY, Linköping University

Division of Vehicular Systems
Department of Electrical Engineering
Linköping University
SE-581 83 Linköping, Sweden

Copyright © 2017 Carl Vilhelmsson

Abstract

The high demands on low fuel consumption and low emissions on the combustion engines of both today, and the future, is highly dependent on advanced control systems in order to fulfill these demands. The control systems and strategies are based on models which describe the physical system. The more accuratly the models describe the real world system, the more accurate the control will be, leading to better fuel economy and lower emissions.

This master's thesis investigates and improves the mass flow model used for a compressible restriction, such as over the throttle valve, EGR valve, or the wastegate valve, for example. The standard model is evaluated and an improvement is proposed which does not assume isentropic flow. This seems to explain the deviation from the isentropic Ψ-function shown in earlier research such as (Andersson, 2005). Furthermore a throttle valve is analyzed in ANSYS in order to show the generation of entropy. The presence of pressure pulsations in a combustion engine is also evaluated, especially how they effect the otherwise assumed steady flow model. It is tested if a mean value pressure is sufficient or if one needs to take the pulsations in to account, and the result shows that a mean pressure is sufficient, at least for the throttle when typical intake manifold pulsations is present. A dynamic flow model is also derived which can be useful for pressure ratios close to one. The dynamic flow model is based on the standard equation but with an extra dynamic term, however it is not implemented and tested due to complexity and time limitation. The proposed new non-isentropic flow model has proven promising and can hopefully lead to lower emissions and better fuel economy.

Acknowledgments

First of I would like to express my gratitude to Lars Eriksson at vehicular system, Linköping University and the air charge group at Volvo Car Corporation which brought this subject to my attention and gave me the opportunity to conduct this master's thesis. Furthermore i would like to thank my supervisor at Linköping University, Robin Holmbom for his guidance and the productive discussions we had. I also want to send a thank to my supervisors at Volvo Car Corporation, Samuel Alfredsson and Marcus Rubensson which have shown great interest and have helped me a lot with supplying me with data and answering questions. A thank also goes out to Tobias Lindell working at the engine lab at Vehicular Systems, Linköping University, helping me with for instance collecting data and installing new sensors on the engine rig.

Linköping, june 2017
Carl Vilhelmsson

Contents

1 Introduction **1**
1.1 Background 1
1.2 Problem Formulation 2
1.3 Expected Results 3
1.4 Outline 4

2 Related Research **5**
2.1 Common Fluid Science 5
2.2 Incompressible Flow Restriction 6
2.3 Compressible Flow Restriction 6
2.4 Pressure Pulsations 7
2.5 Applications for the Flow Model 9
  2.5.1 Wastegate 9
  2.5.2 Throttle and EGR 10
  2.5.3 Turbo 10
  2.5.4 Cylinder Air Charge 11

3 Theory and Phenomena **13**
3.1 Steady Isentropic Compressible Flow 13
3.2 Steady Non-Isentropic Compressible Flow 16
3.3 Pulsating Pressure Ratio 20
3.4 Unsteady Isentropic Compressible Flow 21

4 Approach **25**
4.1 Steady Compressible Flow 26
  4.1.1 Approach 26
  4.1.2 Measurements 27
4.2 Unsteady Compressible Flow 28
  4.2.1 Approach 28
  4.2.2 Measurements 30

5 Results **31**
5.1 Fixed Throttle Position 31

5.2 Normal and Extended Ψ-function 32
5.2.1 Engine Measurements 32
5.2.2 Flow Bench Measurements 35
5.3 Pulsating Pressure Ratio 38
5.4 Throttle Valve ANSYS Analysis 42
5.5 Dynamic Compressible Flow 45

6 Conclusion 53
6.1 Summary 53
6.2 Future Work 55
6.2.1 Ψ-function 55
6.2.2 Dynamic Flow Model 55

A Calculations for Isentropic Compressible Flow 59

B Calculations for Non-isentropic Compressible Flow 63

C Calculations for Unsteady Compressible Flow 67

Bibliography 71

PARAMETERS AND VARIABLES

Notation	Description
p	Pressure [pa]
T	Temperature [K]
$\dot{m}$	Mass flow [kg/sec]
R	Gas constant air [-]
γ	Ratio of specific heats air [-]
ρ	Density [kg/m^3]
V	Velocity [m/s]
h	Enthalpy [KJ/Kg]
c_p	Specific heat constant pressure [kJ/kgK]
c_v	Specific heat constant volume [kJ/kgK]
s	Entropy [kJ/kgK]

ABBREVIATIONS

Abbreviations	Description
VCC	Volvo Car Corporation
VNT	Variable Nozzle Turbine
PID	Proportional Integral Derivateive
CFD	Computational Fluid Dynamics
MVEM	Mean Value Engine Model
EGR	Exhaust Gas Recycling
MATLAB	Calculation program
SIMULINK	Simulation program
ANSYS	Finite element method calculation program
FILTFILT	Filtering function in MATLAB
LSQCURVEFIT	Least square function in MATLAB

1

Introduction

A short introduction to the problems and why it is interesting to investigate them further is presented in this chapter. The main goals and the primary expected results of the thesis along with the outline is also introduced here.

1.1 Background

Today's vehicles have to be more and more environmentally friendly, one of the main effects a vehicle has on the environment is the release of greenhouse gases coming from the burning of fossil fuel. To reduce this effect and save money the consumer wants fuel efficient vehicles. In order to design and control these new engines, models for each component are required to be accurate and reliable in all driving situations. Some of these components are the different valves which directs flows in the engine, such as the throttle, EGR, and wastegate. One aspect that has not been investigated is the effect of pulsations for both low and high pressure ratios.

One example is the wastegate, a bypass valve that controls how much of the exhaust flow goes in to the turbocharger thereby boosting the engine with air leading to better fuel economy. The wastegate flow model is not well developed due to the harsh and unsteady conditions in the exhaust, making it hard to measure the flow and get an accurate model for all working conditions. The model for the wastegate effects the whole engine simulation model. Some of the obvious benefits of having an accurate model is that together with a turbocharger model one can apply a good feed forward to the boost control loop increasing driveability. An accurate model will estimate the exhaust manifold pressure more correctly which affect the calculations for volumetric efficiency, hence correct air fuel ratio will be obtained and lower emissions achieved. This master's thesis will address some different flow phenomena, pulsating and unsteady flow, low and high pressure ratios over restrictions and hopefully end up with an extended useful model for mass flow through a compressible restriction.

1.2 Problem Formulation

Accurate and faster engine control systems are one way to increase fuel economy, driveability, and decrease emissions. For this, better models of the different components in the engine are needed. The wastegate can be seen as a compressible restriction, just as the throttle, and in some cases the EGR-valve. There are two main types of EGR systems, low pressure route, and high pressure route. High pressure route can be seen as a compressible restriction but the low pressure route EGR-valve have to be investigated further. There are several problems when trying to model the wastegate and EGR flow. When using the same analogy as for the throttle, measuring the mass flow can not be done due to the heat which a regular mass flow meter can not handle, and for the EGR the pulsating flow sometimes leads to back flow. The fact that the mass flow is split up between the turbine and the wastegate makes the mass flow meter on the intake side of the engine unusable in order to obtain the mass flow past the wastegate. The pulsations coming from the cylinder when an exhaust valve opens makes the pressure ratio over the wastegate not to be steady which is assumed in the throttle case. There might also be flow disturbances and circulations occurring due to the fact that wastegate and turbine is located so close to each other. Some previous works such as Andersson (2005),Hendricks et al. (1996) have shown that the model used, based on isentropic compressible flow does not correspond with measured data see figure 1.1. That model is then adapted to fit the measured data in many different ways, some different ideas are proposed by for example (Hendricks et al., 1996)(Reshaping $\Psi(\Pi)$-function with help of 2 parameters),(Andersson, 2005)(Uses gamma as tunable parameter). The interesting part is why it differs from the theory, this will be investigated further. To be carried out in this thesis are the following:

- 1: Repeat the measurements in (Andersson, 2005) showing that the $C_d\Psi(\Pi) \neq \Psi(\Pi)$.
- 2: Investigate with the help of CFD to why these phenomena occurs.
- 3: Investigate the effects pressure pulsations have on the model where the conditions otherwise are assumed steady.
- 4: Create an extended flow model, combining the model for an isentropic compressible restriction with the previous investigations.
- 5: Investigate the improvements of the new extended model against the basic model.

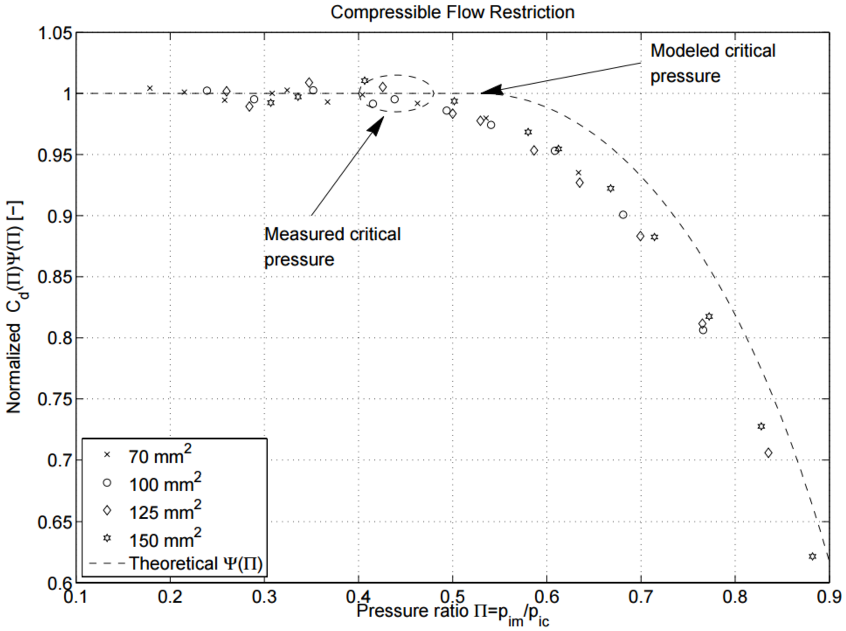

Figure 1.1: *The original data measured by Per Andersson at vehicular system, Linköping University is shown in this figure. One can clearly see the deviation between model and collected data. The original picture comes from (Andersson, 2005).*

1.3 Expected Results

The main expected result of this thesis is an useful extended model for the mass flow through a variable restriction, that can be used for improving the total engine model, which would lead to better and more accurate engine control. This is obtained by closer investigation of the different sub problems.

- 1: Reconstructed measurements from the work in (Andersson, 2005) showing that the theory for an isentropic compressible restriction do not match the measurements.

- 2: CFD simulations trying to explain why the deviation in the $\Psi(\Pi)$-function occurs.

- 3: Plots and data showing the effects a pulsating pressure have on the compressible flow model.

- 4: Flow through a variable restriction is measured for different pressures in a test bench in order to eliminate the effects pulsations have on the mass flow and furthermore evaluating what is causing the deviation.

- 5: Taking the results from the previous stated excepted results and developing a new extended mass flow model.
- 6: Presented measurements of the flow through a restriction and comparing the new extended model against a basic model.

1.4 Outline

The main chapters of this thesis with a short description are as follows:

- **Chapter 1 - Introduction**
  Introduction to the problem, why it is desirable to solve and expected results
- **Chapter 2 - Related Research**
  Presenting the literature studies made on the subject.
- **Chapter 3 - Theory and Phenomena**
  Different theories and ideas are presented in what manner some problems are to be solved.
- **Chapter 4 - Approach**
  This chapter describes how the different tests are to be carried out and what data is to be collected and why.
- **Chapter 5 - Result**
  This presents the results from the different problems and tests stated in previous chapters.
- **Chapter 6 - Conclusion**
  The conclusions which can be drawn are presented here along with some ideas for future work.

2

Related Research

Here some related research is presented which were part of the literature studies conducted in order to form a better understanding of the subject of this master's thesis. Information is also collected about both common fluid science and where these equations can be applied when modeling some engine components is presented here.

2.1 Common Fluid Science

Fluid is the common name for gases and liquids, a fluid's properties can for example be described by its viscosity, compression module, and density. These basic properties are also dependent on the internal states of a fluid, such as pressure and temperature, but can in some cases for simplicity be considered as constants. There are three main governing equations within fluid science, the continuity equation which states the preservation of mass, the momentum equation which is a form of newtons second law of motion, the energy equation which states the preservation of energy. When considering a fluid flowing in a pipe one very useful dimensionless number is the Reynold's number which is the relation between inertial forces and viscous forces. The Reynold's number can describe the type of flow, if it is laminar, semi turbulent or fully developed turbulent flow, this is very useful when choosing the approach by which a problem is to be solved. Reynold's number is described in equation (2.1), where U is the relative fluid velocity, L is the characteristic length and v is the dynamic viscosity. For a non-circular pipe the characteristic length (L) is the hydraulic diameter (d_h), described in equation (2.2) where A is the area of the cross section and O is the circumference. More basic fluid science is presented in (Karl Storck, 2012).

$$Re = \frac{Inertialforces}{Viscousforces} = \frac{UL}{v} \tag{2.1}$$

$$d_h = \frac{4A}{O} \tag{2.2}$$

2.2 Incompressible Flow Restriction

An incompressible flow is a flow where the change in density of the fluid is very small and can be neglected. Incompressible flow can be described with the Bernoulli equation, if friction and compressibility effect are neglected. In (Çengel et al., 2012) the incompressible flow equation is derived from Newton's second law of motion. The inertia of the gas when reaching high velocities is the reason the flow is considered to be compressible, when the velocities are low the inertia can be neglected, hence incompressible flow. Equations for such flows through a restriction are described in (Eriksson and Nielsen, 2014) both for laminar and turbulent flows. The long route EGR-valve can perhaps be seen as an incompressible flow since the pressure drop over the valve is low, hence the gas velocity and inertia is low, however in (Klasén, 2016) a compressible flow model is used since it produced a slightly better fit to measured data.

2.3 Compressible Flow Restriction

A compressible flow is a flow where the density in the fluid changes significantly and have to be considered. The flow equations for an isentropic compressible restriction with the shape of a converging nozzle, seen in figure 3.1a, are derived in (Çengel et al., 2012). However, the assumption that these equations apply to the shape of a throttle shown in figure 3.1b, and also the shapes of wastegate and in some cases EGR valves, are made in many automotive works. This assumption might be the reason for the deviation from measured data to theory. Assuming the flow is isentropic, compressible, and adiabatic a model for the throttle is described in (Eriksson and Nielsen, 2014). Since it is in this thesis beneficial to have the $\Psi(\Pi)$ function normalized, to make it easier to compare with normalized data, the normalized model stated in (Andersson, 2005) is to be used. Here also a small linear region is added to fulfil the Lipschitz condition, and prevent oscillations. An indication that the linear region is to small is if oscillations in mass flow occurs during simulations at steady state, stated in (Eriksson and Nielsen, 2014).

Together with others, (Andersson, 2005) says that C_d, the discharge coefficient, are mainly dependent on two factors, pressure ratio Π and the valve angle α. The area dependent factor $C_d(\alpha)$ is hidden within the model for effective area, as in (Eriksson and Nielsen, 2014), $A_{eff}(\alpha) = C_d(\alpha)A(\alpha)$, which are determined using MATLAB function *lsqcurvfit*, hence there is no need to determine $C_d(\alpha)$ solely. To determine if the pressure ratio dependent factor of $C_d(\Pi)$ is negligible, (Andersson, 2005) plots $C_d(\Pi)\Psi(\Pi)$ together with only the $\Psi(\Pi)$-function and here a deviation occurs which implies that $C_d(\Pi)$ can not be ignored. His test is carried out by setting a throttle valve at a fixed position and doing a sweep in pressure ratio, which is done by controlling the engine speed. Furthermore the data is normalized by dividing with the mean of the three biggest measured values for each throttle angle, this to remove the area/angle dependent factor. Explained, the biggest values are assumed to be the same as $A_{eff}(\alpha)$ since $C_d(\Pi)\Psi(\Pi)$ is one where the biggest values occurs, hence a division removes the effect of $A_{eff}(\alpha)$. Further explanation on how this is used is described in the approach chapter.

2.4 Pressure Pulsations

In the books (Ockendon, 2003) and (Lighthill, 2001) waves and compressible flow are described in detail. Special interest for this thesis are longitudinal waves in tubes which can be described using non-linear gas dynamic equations, (2.3). The assumption that the variables only change along the length of the tube is made, for every cross section area the variables are thus the same. These equations are obtained by solving the governing equations, which are the continuity equation, momentum equation, and energy equation. These equations are described further in (Yang, 2015) and (Chalet et al., 2011).

$$\frac{\partial \varphi}{\partial t} + \frac{\partial F(\varphi)}{\partial x} = B \tag{2.3a}$$

$$\varphi = \begin{bmatrix} \rho A \\ \rho u A \\ \rho\left(e + \frac{1}{2}u^2\right)A \end{bmatrix} \tag{2.3b}$$

$$F(\varphi) = \begin{bmatrix} \rho u A \\ (p + \rho u^2)A \\ \rho u\left(e + \frac{1}{2}u^2 + p\rho^{-1}\right)A \end{bmatrix} \tag{2.3c}$$

$$B = \begin{bmatrix} 0 \\ p\frac{dA}{dx} - \rho F_r \\ \rho q e A \end{bmatrix} \tag{2.3d}$$

These equations are preferable solved numerically, but analytical solution exists, however they might only apply to specific conditions. One of those solutions gives the linear acoustic wave equation (2.4), where only small fluctuations in the thermodynamic properties, pressure and density are considered and all non-linear effects are negligible. The mean velocity is not taken into account, all this considered, these equation are a good, if not perfect description for sound waves where all the considerations are true.

$$\frac{\partial^2 p_e}{\partial x^2} = \frac{1}{c_0^2}\frac{\partial^2 p_e}{\partial t^2} \tag{2.4}$$

The aucustic wave equation is useful when considering sound in the engine, but might not be useful when modelling the high amplitude pressure pulsations, and varying gas speed in the exhaust or intake manifold. In the books mentioned above there are also models for waves propagating through restrictions, applying the analogy to electrical impedance and inductance. In (Lighthill, 2001) the inductance is described carefully, and some examples for various geometries are given, it is to be solved with numerical integration of the Laplace equation for that specific geometry, or approximated. Which in the case of a variable restriction makes it very inconvenient, a map for different areas, pressure ratio over restriction, and flow would have to be made to get the correct inductance for all cases. This makes the inductance approach, at least in this case, very inconvenient but for a non-variable restriction and known waves it is useful. However in (Kiwan et al., 2016) an unsteady compressible flow equation is derived which takes the inertia of the gas into account, hence making it possible to take the pulsations and transients into account. This unsteady compressible flow equation seems to estimate the flow much more accurate than the steady compressible flow equation in (Çengel et al., 2012). (Kiwan et al., 2016) validates the model against "GT power", which is an engine simulation program and not real world data, however "GT power" is well recognized among engine manufacturers.

In a combustion engine it is two main type of waves, expansion wave, and compression wave, the expansion wave is a wave of lower pressure such as in the intake manifold and the compression wave is a wave of higher pressure such as in the exhaust manifold. When these waves enters a larger volume or cavity a part of the wave is reflected backwards but as the opposite wave, detailed description in (Lighthill, 2001). For example, a low pressure wave in the intake runner excited by the opening of the intake valve enters the larger manifold cavity and this causes a part of the wave energy to reflect back into the runner as a compression wave. This effect is used when engine designers tune the length of the runners so that the reflected compression wave enters the cylinder just before the intake valves are closing. In many works the waves effect are neglected and only some mean value model is used, however in (Stockar et al., 2016) a way of modelling the transients and waves are proposed which uses the one dimensional wave equations and a reduction methodology to make the equations more manageable. This wave description together with the unsteady compressible restriction equation in (Kiwan et al., 2016) can be useful to both model the waves and calculate their effects on the flow through a restriction. In (Semlitsch et al., 2014) an in depth analysis of the flow leaving the cylinders through the exhaust valves are made, the approach is numerical with finite elements which do not directly help this thesis, but a wider understanding of the different events under which gas enters the exhaust manifold are described. There are two main parts under which gases evacuates the cylinder, the blow-down phase, which occurs when the exhaust valve first opens and the pressure in the cylinder are rapidly blown out until $p_{cyl} = p_{em}$. Part two is when the upward motion of the piston is pushing out the remaining exhaust gases. This is also described in (Eriksson and Nielsen, 2014) where the different events also can be seen in a $p - V$ diagram.

The frequencies of the pulsations are shown in previous works such as (Macián et al., 2004) and (Liang and Holmbom, 2016), where measurements of pressure have been made and proven to be the same as that of the exhaust valves openings (2.5). There will also be resonance frequencies due to the exhaust manifold volume and length of pipe.

$$\omega_p = \frac{2RPM}{60} 2\pi \tag{2.5}$$

In (Thomasson and Eriksson, 2015) a model for the pressure waves in the exhaust manifold are developed, this model assumes exhaust valve as a compressible restriction and calculates the cylinder pressure trace. When the exhaust valves opens the cylinder pressure and temperature are used to calculate the rate of mass flow to the exhaust manifold, hence leading to pressure pulsations in the volume.

2.5 Applications for the Flow Model

The use of an extended flow model taking the pulsations and dynamic behavior into account have many applications where such conditions are present, this thesis focuses on the valves related to combustion engines such as the throttle, wastegate, and EGR valves. In this section a short introduction of the different valves, and improvements an accurate flow model can have is described.

2.5.1 Wastegate

When modeling a valve such as the wastegate valve there are two main parts, the signal to position model, and the position to flow model. More about modelling, both with a system identification approach and a physical modelling approach are described in (Ljung and Glad, 2004).

Flow Model

The flow model is using the above described compressible flow through restriction equations, where the $A_{eff}(\alpha)$ and $C_d(\Pi)$ are to be found. This assumes that the discharge coefficient can be divided into two parts one angle dependent and one pressure ratio dependent, $C_d(\alpha, \Pi) = C_d(\alpha)C_d(\Pi)$. Starting of with the modelling of the $C_d(\Pi)\Psi(\Pi)$-function one can chose between some different approaches described in for example (Andersson, 2005), and (Hendricks et al., 1996). However the idea is the same, normalizing the function to remove area dependent factor and then fitting $C_d(\Pi)$ so that $C_d(\Pi)\Psi(\Pi)$ agrees with measurements. When $C_d(\Pi)\Psi(\Pi)$ are modeled, the approach in (Eriksson and Nielsen, 2014) can be used to model the A_{eff} using *lsqcurvfit* to parametrize some polynomial function. Measurements are obviously made in order to obtain the data for fitting the models.

Position Model

The modelling of the positioning in such a valve as the wastegate are carefully described in (Thomasson et al., 2013) with help of, for example (Mehmood et al., 2010) to model the aerodynamic force. First a model for signal to wastegate actuator are made with slow ramps to describe the statics and then steps are made to evaluate the time constant, there are different time constants depending on if pressure is rising or falling. Furthermore according to Newton's second law of motion a force balance is set up (2.6), which is the model for the wastegate's position.

$$\ddot{x}m = F_{amb} - \dot{x}b - F_{act} - F_{fr} - F_{sb} - F_{aero} \tag{2.6}$$

An approach by which the different forces are identified is described, first by static experiment to remove the influence of dynamic friction and the mass, when they are identified steps are made and the mass (m) and dynamic damping (b) are fitted using *lsqcurvfit*. The aerodynamic force is modeled in (Mehmood et al., 2010) for a VNT-system but the approach may be the same. The aerodynamic force is mainly dependent on the pressure difference between the exhaust manifold and the following exhaust. Previous forces are calculated with engine off to remove the influence of aerodynamic force, when engine is turned on the difference between the expected static position and the real position are due to aerodynamic force which then can thus be determined. A model for the vacuum tank and pump is also proposed in (Thomasson et al., 2013). However assuming that the vacuum pump can keep the pressure constant, a vacuum reference pressure will suffice. A model for the wastegate position is needed in order to obtain a good feed forward to the turbo control, and be able to evaluate the improvements of a better flow model.

2.5.2 Throttle and EGR

The throttle and EGR valves are very similar in the design but have different purposes, throttle controlling the air flow into the engine and the EGR controlling how much exhaust gases are recycled. Both valves are however butterfly valves controlled with a servo motor, the design can be seen in figure 3.1b. The positioning system of these valves are much simpler to model than the positioning of the wastegate valve since they are actuated by, in most cases, a closed loop servo motor. In (Eriksson and Nielsen, 2014) a first order system is proposed for the throttle reference signal to position, a simple step response is sufficient to obtain the gain and time constant. The flow modeling is furthermore the same as for the wastegate, however a different polynomial function for the effective area (A_{eff}) might be used to capture the different shape characteristics.

2.5.3 Turbo

The boost pressure control system are greatly dependent on estimation and modelling of the turbocharger, which in turn needs an accurate estimation of mass flow through the turbine driving the turbo charger. The difficulty lies here in estimating how the total mass flow is divided among the turbine and the wastegate path. If accurate models for wastegate signal to boost pressure are presented a fast control system can be developed. First when designing a control system for the boost pressure, models for the compressor, turbine, and connecting shaft is needed. In (Eriksson and Nielsen, 2014) basic models for compressor, turbine, and shaft are described, in (Leufvén and Eriksson, 2013) an extension of these models are proposed that is choke and surge capable. Furthermore in (Llamas and Eriksson, 2017) a new way of fitting the data to the models is described, where not the model error is minimized, instead the orthogonal distance to the model is minimized. In (Leufven and Eriksson, 2016) turbo compressor models are extended for low pressure ratios. There are many different approaches on how to develop a turbo control system depending on such as what sensors are available and how much effort is put into the design. In (Eriksson and Nielsen, 2014) a static feed forward from a look up table, together with a second order engine speed dependent system is used. The look up table is the static gain from wastegate position to boost pressure for different engine speeds, and the second order systems are identified with help of step responses, also for different engine speeds. The regulator parameters, which also are engine speed dependent, are tuned using IMC. In (Criscuolo et al., 2011) a similar approach is made, however it is for a two stage sequential turbocharging system and the supply voltage is compensated for. In (Liang and Holmbom, 2016) a structure where the system is modeled in different stages are made, here sensors for turbo speed and wastegate position is supplied. Different solutions are proposed on how to model the system for requested boost pressure to requested turbo speed, a look up table, non-linear static compensator, or physical modeling. The turbo speed is then controlled instead of controlling the boost pressure directly. Static errors are removed by a feedback controller from boost pressure to requested turbo speed. The system from wastegate to turbo speed is then identified by doing step responses and assuming first order system. This way parts of the system can be modeled separately, and hopefully leading to a better and more complete definitive model, due to the fact that less characteristics of different parts are overlooked. In common for most turbo controllers are that they consists of some sort of PID-controller, however there are exceptions, such as in (Liang and Holmbom, 2016) where a state feedback is used with an integrating part. Common is also the use of kalman filters to estimate states which are of interest. More general control theory can be read about in (Glad and Ljung, 2006), (Glad and Ljung, 2003), and (Martin Enqvist and Strömberg, 2014), for example.

2.5.4 Cylinder Air Charge

The total air mass flow to the cylinder are described in (Andersson, 2005) (2.7), here for one cylinder, which then is used to calculate the correct amount of fuel to be injected. The volumetric efficiency η_{vol}-function are described in many different works and in many different ways, it is usually a function which is parametrized with regards to engine speed and intake manifold pressure, some models are proposed in (Eriksson and Nielsen, 2014).

$$CAC = \eta_{vol} \frac{p_{im} V_d}{R_{im} T_{im}} \tag{2.7}$$

There is also the approach of physical modeling where effects as charge cooling, residual gases, and fuel enrichment are taken into account. One such model (2.8) are described in (Andersson, 2005), here it is only two tuning parameters, and the η_{vol}-function is not present.

$$CAC = \frac{p_{im}}{R_{im}\left(T_{im} - C_1 \frac{1-\lambda^2}{\lambda^2}\right)} C_{\eta_{vol}} \frac{\left(r_c - \left(\frac{p_{em}}{p_{im}}\right)^{\frac{1}{\gamma_e}}\right) V_d}{\left(1 + \frac{1}{\lambda\left(\frac{A}{F}\right)_s}\right)(r_c - 1)} \tag{2.8}$$

A sensitivity function for how the exhaust pressure p_{em} effects the CAC is also derived from (2.8) in (Andersson, 2005), which is a good tool when evaluating how much the improved estimations of p_{em} due to better wastegate flow model, effects the CAC. In order to compare the improvements of the flow model a baseline exhaust pressure model is required which also is presented in (Andersson, 2005).

3

Theory and Phenomena

In this chapter the theory and governing equations behind the models used in this master's thesis are presented. The assumptions made when deriving the models are explained and ways of improving and investigating why some errors occur are described here.

3.1 Steady Isentropic Compressible Flow

Similar derivation is made in a lots of previous works, one example (Çengel et al., 2012), but the derivation is also presented her in order for the reader to get a better understanding. In steady flow, a flow where the fluid properties can change from point to point, but for every point they do not change with time. The conservation of energy equation, with help of the enthalpy describing internal energy can be applied, assuming no work or heat is transfered out, or in to the system. The following equation can be stated:

$$h_1 + \frac{V_1^2}{2} + gz_1 = h_2 + \frac{V_2^2}{2} + gz_2 \tag{3.1}$$

For an ideal gas the enthalpy is only dependant on the temperature, when assuming that the specific heat constant pressure (c_p) is a constant, hence the following equation applies:

$$h_2 - h_1 = c_p(T_2 - T_1) \tag{3.2}$$

Studying the figure 3.1 and assuming that it is only small changes in potential energy, ($z_1 - z_2 \approx 0$). Also assuming that the inlet velocity is very low relative to the exit velocity $V_2^2 - V_1^2 \approx V_2^2$ Combining this assumption with previous equations (3.1) and (3.2) following equation is obtained:

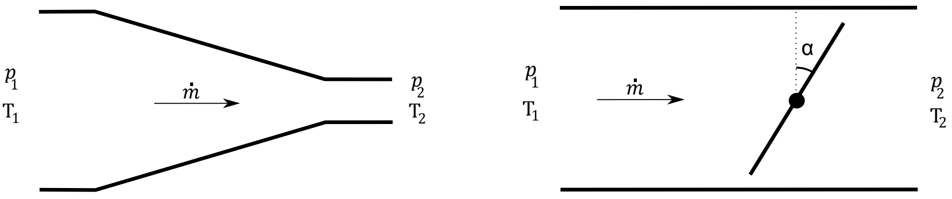

(a) *Converging nozzle which the isentropic compressible restriction equations is derived for.*

(b) *A throttle body which the isentropic compressible restriction equations is applied on.*

Figure 3.1: *Assuming steady and isentropical flow makes the equations apply to both cases.*

$$T_1 = T_2 + \frac{V_2^2}{2c_p} \tag{3.3}$$

Assuming isentropic process for an ideal gas, following equation applies:

$$\frac{T_2}{T_1} = \left(\frac{p_2}{p_1}\right)^{\frac{(\gamma-1)}{\gamma}} \tag{3.4}$$

Introducing the Mach number for air which is a ratio of the velocity and the local speed of sound (c).

$$M = \frac{V}{c} = \frac{V}{\sqrt{\gamma R T}} \tag{3.5}$$

Replacing the velocity with the Mach number in the equations (3.3) and (3.4) these new equations are obtained, see appendix A for further description of calculations.

$$\frac{T_1}{T_2} = 1 + \frac{\gamma - 1}{2} M^2 \tag{3.6}$$

$$\frac{p_1}{p_2} = \left(1 + \frac{\gamma - 1}{2} M^2\right)^{\frac{\gamma}{\gamma-1}} \tag{3.7}$$

The mass flow air can be described as follows, with the help of the ideal gas law, and the previous stated equations (3.7), and (3.6), see appendix A for further explained calculations:

$$\dot{m}_{ideal} = \rho A V \tag{3.8}$$

Replacing the temperature and pressure after the nozzle with the pressure before gives:

$$\dot{m}_{ideal} = \frac{p_1}{\sqrt{R T_1}} A M \sqrt{\gamma} \left(1 + \frac{\gamma - 1}{2} M^2\right)^{-\frac{(\gamma+1)}{2(\gamma-1)}} \tag{3.9}$$

Substituting the Mach number with pressure ratio (Π), see appendix A, adding the discharge coefficient ($C_d(\alpha, \Pi)$) which we assume is depending on the throttle angle and pressure ratio. Also changing the area factor (A) to a function of throttle angle ($A(\alpha)$) seen in figure 3.1b. This sets up for a useful function when applied to a variable nozzle, valve, or throttle.

$$\dot{m} = \frac{p_1}{\sqrt{RT_1}} A(\alpha) C_d(\alpha, \Pi) \underbrace{\sqrt{\frac{2\gamma}{\gamma - 1}\left(\Pi^{\frac{2}{\gamma}} - \Pi^{\frac{\gamma+1}{\gamma}}\right)}}_{\Psi(\Pi)} \tag{3.10}$$

Where Π is the ratio of pressure over the nozzle if flow is going from pressure one to pressure two, otherwise the pressure and temperature in the equation have to be switched so that the ones upstream are used in equation (3.10). Assuming only one direction of mass flow the pressure ratio are defined as follows:

$$\Pi = \begin{cases} \frac{p_2}{p_1} & \text{if} \quad p_2 < p_1 \\ 1 & otherwise \end{cases} \tag{3.11}$$

The critical pressure ratio is at the maximum of the $\Psi(\Pi)$-function, this happens when the speed of sound is reached in the nozzle, this occurs for pressure ratios:

$$\Pi = \left(\frac{2}{\gamma + 1}\right)^{\frac{\gamma}{\gamma-1}} \tag{3.12}$$

Using the critical pressure ratio in the Ψ-function we state the normalized Ψ^*-function as follows:

$$\Psi^*(\Pi) = \frac{\sqrt{\frac{2\gamma}{\gamma-1}\left(\Pi^{\frac{2}{\gamma}} - \Pi^{\frac{\gamma+1}{\gamma}}\right)}}{\sqrt{\frac{2\gamma}{\gamma-1}\left(\left(\frac{2}{\gamma+1}\right)^{\frac{2}{\gamma-1}} - \left(\frac{2}{\gamma+1}\right)^{\frac{\gamma+1}{\gamma-1}}\right)}} \tag{3.13}$$

Applying the linear region in order to fulfil the Lipschitz condition and prevent oscillations for pressure ratios near one when simulating, also setting the values under the critical pressure ratios to one. This in order for the model to work in al possible conditions.

$$\Psi(\Pi) = \begin{cases} 1 & \text{if} \quad 0 < \Pi \leq \left(\frac{2}{\gamma+1}\right)^{\frac{\gamma}{\gamma-1}} \\ \Psi^*(\Pi) & \text{if} \quad \left(\frac{2}{\gamma+1}\right)^{\frac{\gamma}{\gamma-1}} < \Pi \leq \Pi_{lin} \\ \Psi^*(\Pi_{lin})\frac{\Pi-1}{\Pi_{lin}-1} & \text{if} \quad \Pi_{lin} < \Pi \leq 1 \end{cases} \tag{3.14}$$

This function can be seen in the figure 3.2 where the linearized limit is set to $\Pi_{lin} = 0.99$ and $\gamma = 1.4$.

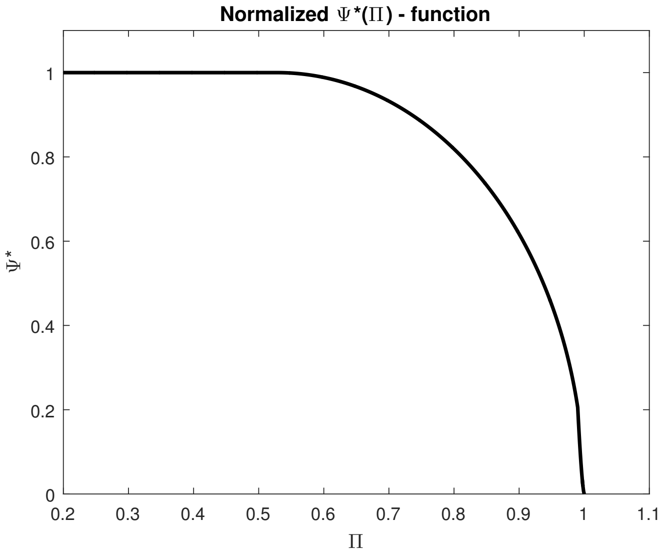

Figure 3.2: *Here the* Ψ*-function for an isentropical compressible nozzle can be seen with both linearized area for pressure ratios over* 0.99*, and for pressure ratios below the critical ratio the function are set to one.*

3.2 Steady Non-Isentropic Compressible Flow

Previous calculations of the expansion and acceleration were based on equation (3.4) which assumes the generated entropy to be zero. Entropy is a state property, entropy is the quantity of microscopic disorder in a system, more information about entropy can be found in (Çengel et al., 2012). The change of entropy is defined as follows:

$$dS = \left(\frac{dQ}{T}\right) \tag{3.15}$$

For an ideal gas where the specific heats are assumed constants, the change in entropy can be described as follows for any process:

$$s_2 - s_1 = c_v ln\frac{T_2}{T_1} + Rln\frac{V_1}{V_2} \tag{3.16a}$$

$$s_2 - s_1 = c_p ln\frac{T_2}{T_1} - Rln\frac{p_2}{p_1} \tag{3.16b}$$

If the process is assumed to be isentropic ($s_2 - s_1 = 0$) the equation (3.16b) gives the previous stated equation (3.4). In figure 3.3, a diagram of the isentropic process is shown together with a more accurate process which is called the actual process. A logical explanation to the loss of kinetic energy which can be seen in the diagram is the fact that the molecules bounce and collide lowering the overall kinetic energy and thus generating entropy, and internal energy in the form of temperature. The temperature drop will thus be a bit lower than the theoretical isentropical calculated temperature.

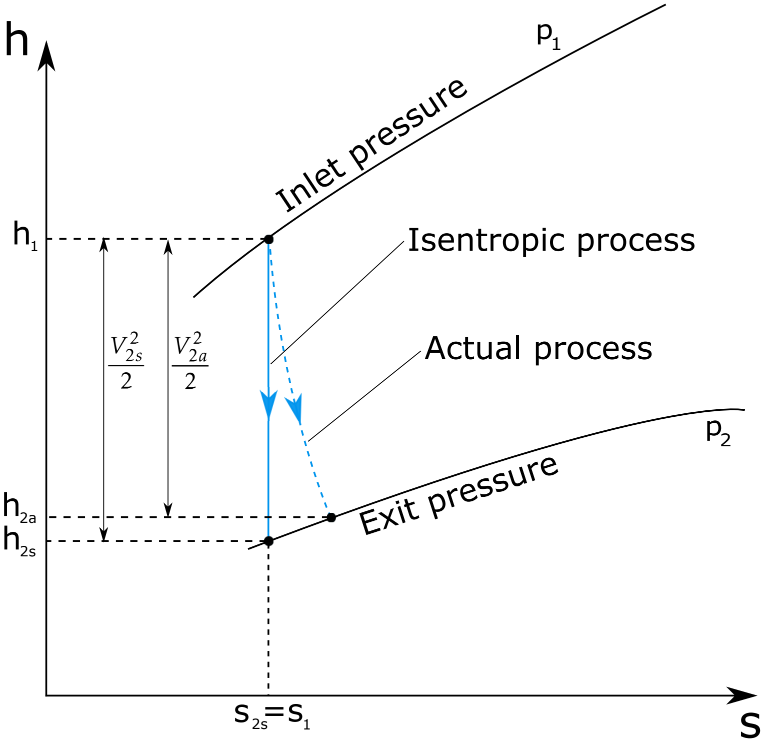
h
p1
Inlet pressure
h1
Isentropic process
$\frac{V_{2s}^2}{2}$
$\frac{V_{2a}^2}{2}$
Actual process
p2
Exit pressure
h2a
h2s
s2s=s1
s

Figure 3.3: The entropy on the x-axis and the enthalpy on the y-axis. A throttling process is shown, for both isentropic process where the entropy is constant hence equation (3.4) *does apply, and one actual process where the entropy increase and thus also the enthalpy which leads to lower exit velocity and lower mass flow.*

The efficiency of a nozzle, or some other restriction over which there is a pressure drop, is defined as:

$$\eta_N = \frac{V_{2a}^2}{V_{2s}^2} \tag{3.17}$$

The kinetic energy equation (3.3) still applies but the isentropic equation (3.4) does not, however the isentropic relation with regard to the efficiency of the nozzle can be stated as follows, which is shown in appendix B.

$$\frac{T_{2a}}{T_1} = 1 - \eta_N \left(1 - \left(\frac{p_2}{p_1}\right)^{\frac{\gamma-1}{\gamma}}\right) \tag{3.18}$$

This new governing equation leads to a different result for the mass flow which in this case takes the isentropic efficiency into account, the calculations are shown in appendix B and the resulting equation below. The pressure ratio is corrected to make the calculations easier, this corrected pressure ratio (or more accurate the temperature ratio) is called $\Pi_{\eta N}$ and is defined in both appendix B and equation (3.19).

$$\Pi_{\eta_N} = 1 - \eta_N\left(1 - \left(\frac{p_2}{p_1}\right)^{\frac{\gamma-1}{\gamma}}\right) \tag{3.19}$$

$$\dot{m}_{full} = \frac{p_1}{\sqrt{RT_1}} A(\alpha) C_d \sqrt{\frac{2\gamma}{\gamma-1}\left(\Pi_{\eta_N}^{\frac{2}{(\gamma-1)}} - \Pi_{\eta_N}^{\frac{(\gamma+1)}{(\gamma-1)}}\right)} \left(\frac{\eta_N}{(\eta_N - 1)\frac{1}{\Pi_{\eta_N}} + 1}\right)^{\frac{\gamma}{\gamma-1}} \tag{3.20}$$

$$\Psi = \sqrt{\frac{2\gamma}{\gamma-1}\left(\Pi_{\eta_N}^{\frac{2}{(\gamma-1)}} - \Pi_{\eta_N}^{\frac{(\gamma+1)}{(\gamma-1)}}\right)} \left(\frac{\eta_N}{(\eta_N - 1)\frac{1}{\Pi_{\eta_N}} + 1}\right)^{\frac{\gamma}{\gamma-1}} \tag{3.21}$$

One can see that the critical pressure ratio does not occur at the same pressure ratio as for isentropic flow, the pressure ratio is now a function of the isentropic efficiency. The critical pressure ratio is easiest obtained by finding the maximum value of the Ψ-function numerically. The normalized pressure ratio function is thus:

$$\Psi^* = \frac{\sqrt{\frac{2\gamma}{\gamma-1}\left(\Pi_{\eta_N}^{\frac{2}{(\gamma-1)}} - \Pi_{\eta_N}^{\frac{(\gamma+1)}{(\gamma-1)}}\right)} \left(\frac{\eta_N}{(\eta_N-1)\frac{1}{\Pi_{\eta_N}}+1}\right)^{\frac{\gamma}{\gamma-1}}}{\max(\Psi)} \tag{3.22}$$

However for low isentropic efficiencies the Ψ-function will never reach a critical pressure ratio before $\Pi \approx 0$, the Ψ-maximum for low isentropic efficiencies is reached for pressure ratios close to zero.

$$\lim_{\Pi \to 0} \Psi = \inf \text{ for } \eta_N \lessapprox 85\% \tag{3.23}$$

This is inconvenient when the function is to be normalized for low efficiencies, one can thus remove the lowest pressure ratios in order to not divide with an extremely large number and ruining the possibility of comparing the shapes of the Ψ-function for the different efficiencies. The critical pressure ratio as a function of the isentropic efficiency is shown in figure 3.5. In (Çengel et al., 2012) it is stated that the efficiency of a nozzle or other short restriction is in most cases above 90% and for converging nozzles above 95%.The previously constant critical pressure ratio is now replaced with the new efficiency dependent critical pressure ratio, defined as the pressure ratio where the Ψ-function reaches maximum.

$$\Psi(\Pi_{crit}, \eta_N) = \max(\Psi) \tag{3.24}$$

$$\Psi(\Pi) = \begin{cases} 1 & \text{if} \quad 0 < \Pi \leq \Pi_{crit} \\ \Psi^*(\Pi) & \text{if} \quad \Pi_{crit} < \Pi \leq \Pi_{lin} \\ \Psi^*(\Pi)\frac{\Pi - 1}{\Pi_{lin} - 1} & \text{if} \quad \Pi_{lin} < \Pi \leq 1 \end{cases} \tag{3.25}$$

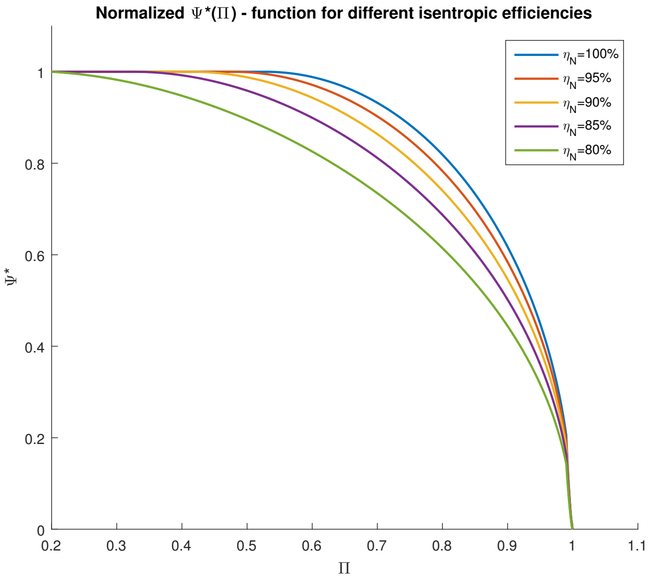

Figure 3.4: *Here the* Ψ*-function for various isentropical efficiencies over a nozzle can be seen with both linearized area for pressure ratios over* 0.99*. Also for pressure ratios below the critical ratio the function are set to one.*

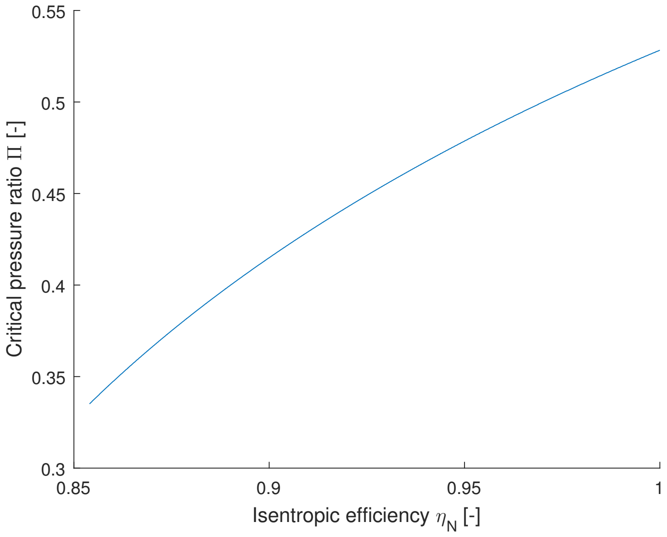

Figure 3.5: *Here the critical pressure ratio is shown as a function of the isentropic efficiency, worth noting is that for efficiencies below* 85% *there is no critical pressure ratio since the extended* Ψ*-function does not have a maximum value here as stated in equation* (3.23)

3.3 Pulsating Pressure Ratio

The use of a mean pressure ratio when calculating the momentarily mass flow can be one factor that effects the deviating shape of the Ψ-function. Since the Ψ-function is non-linear the assumption that the average pressure ratio can be used to calculate the mean Ψ-function value is incorrect but might be sufficient. The assumption is explained in figure 3.6.

$$\Psi = \begin{cases} \Psi(mean(\Pi)) & \text{assumption which is used.} \\ mean(\Psi(\Pi)) & \text{correct way.} \end{cases} \tag{3.26}$$

For pulsating flows this assumption would in theory distort the Ψ-function in the same way as is shown in (Andersson, 2005) where the real Ψ-values is a bit under the theoretical Ψ-function. However if the intake pulsations is large enough to explain the deviation or if it is the isentropic efficiency which causes this effect needs to be investigated further.

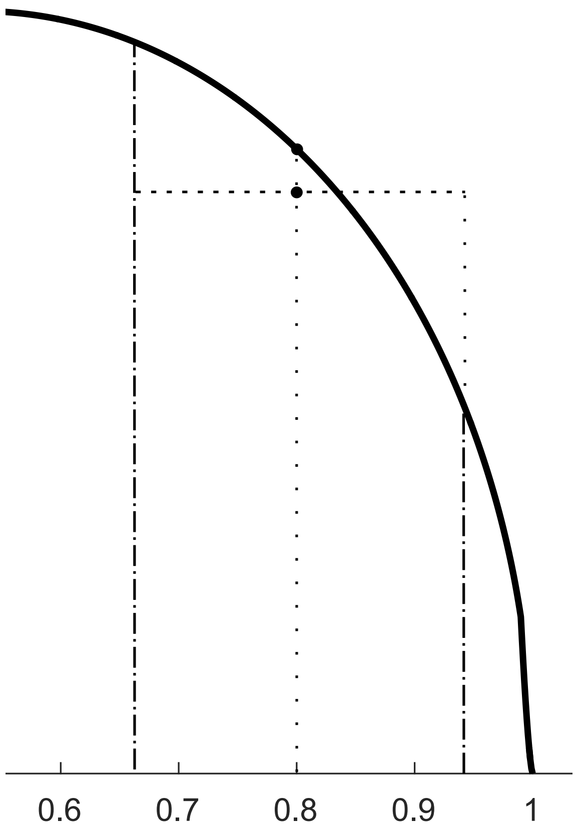

Figure 3.6: *If the pressure ratio is pulsating between the two outer dashed lines and the mean pressure ratio is the dotted line, using the mean pressure ratio to calculate the* Ψ*-value one gets the upper dot on the* Ψ*-function line. The correct way to calculate the average* Ψ*-value is for every time step calculate the* Ψ*-function value and then take the average of these. The lower dot is thus obtained, the difference is shown in equation* (3.26)

3.4 Unsteady Isentropic Compressible Flow

Using Newton's second law of motion on a fluid particle in an unsteady compressible flow, and neglecting the gravity, which often can be done assuming small height differences in the flow, one gets the 1-D linear momentum equation, derivation shown in appendix C.

$$\frac{1}{\rho}\frac{\partial p}{\partial x} + v\frac{\partial v}{\partial x} + \frac{\partial v}{\partial t} = 0 \tag{3.27}$$

Assuming isentropic processes in the flow the isentropical relation between density and pressure, can be used to substitute the density in equation (3.27) with a stagnation/inlet density and pressure.

$$\frac{\rho}{\rho_0} = \left(\frac{p}{p_0}\right)^{\frac{1}{\gamma}} \tag{3.28}$$

$$\frac{1}{\rho_0}\left(\frac{p_0}{p}\right)^{\frac{1}{\gamma}}\frac{\partial p}{\partial x} + v\frac{\partial v}{\partial x} + \frac{\partial v}{\partial t} = 0 \tag{3.29}$$

Applying the equation to a restriction in a pipe, the assumption that the variables only change with the length of the pipe but is the same for every cross section area is to be made. The flow is thus uniform, and have only one dimension, hence the above equation (3.29) applies. The equation also assumes isentropic flow, this is motivated by the small effect the isentropic efficiency have when pressure ratio is close to one, where this model is intended for use. Further integrating the equation from the start of the pipe x_0 where the pressure is p_0 to x_t and pressure p_t, t, indicating the throat of the valve. Also assuming that the inlet velocity is negligible $v_0 \approx 0$ the integration becomes:

$$\frac{p_0^{\frac{1}{\gamma}}}{\rho_0}\int_{x_0}^{x_t}\frac{1}{p^{\frac{1}{\gamma}}}dp + \frac{v_t^2}{2} + \int_{x_0}^{x_t}\frac{\partial v}{\partial t}dx = 0 \tag{3.30}$$

Further simplifications and assumptions of the equation above, shown in appendix C, gives an unsteady compressible mass flow equation where an extra dynamic term is added to the previous steady equation. Similar assumptions and calculations as in appendix C are made in (Kiwan et al., 2016)

$$A_{eff}^2 C_d^2 \frac{p_0^2}{T_0 R}\frac{2\gamma}{\gamma - 1}\left(\Pi^{\frac{2}{\gamma}} - \Pi^{\frac{\gamma+1}{\gamma}}\right) = \dot{m}^2 + A_{dyn}A_{eff}^2 C_d^2 \frac{2p_0}{T_0 R}\Pi^{\frac{2}{\gamma}}\frac{\partial \dot{m}}{\partial t} \tag{3.31}$$

In order to deal with the possibility of reversing mass flows some comparisons are to be made in order to determine in which direction the pressure ratio forces the flow. The flow does not necessary flow from high pressure to low pressure since the inertia of the flow can force flow from low to high pressure.

$$p_o = \begin{cases} p_1 & \text{if} \quad p_1 \geq p_2 \\ p_2 & \text{if} \quad p_1 < p_2 \end{cases} \tag{3.32}$$

$$T_o = \begin{cases} T_1 & \text{if} \quad p_1 \geq p_2 \\ T_2 & \text{if} \quad p_1 < p_2 \end{cases} \tag{3.33}$$

$$\Pi = \begin{cases} \frac{p_2}{p_1} & \text{if} \quad p_1 \geq p_2 \\ \frac{p_1}{p_2} & \text{if} \quad p_1 < p_2 \end{cases} \tag{3.34}$$

The mass flow direction is of interest and needs to be determined, the equation only states the magnitude. To ensure this effect is described the steady part of the equation have to change sign when the flow is driven from p_2 to p_1 if the positive flow is defined from p_1 to p_2. The mass flow square are to be divided into two parts, one with absolute sign, to prevent the square from removing the sign dependency.

$$sign(p_1 - p_2) A_{eff}^2 C_d^2 \frac{p_0^2}{T_0 R} \frac{2\gamma}{\gamma - 1} \left(\Pi^{\frac{2}{\gamma}} - \Pi^{\frac{\gamma+1}{\gamma}} \right) = \dot{m}|\dot{m}| + A_{dyn} A_{eff}^2 C_d^2 \frac{2p_0}{T_0 R} \Pi^{\frac{2}{\gamma}} \frac{\partial \dot{m}}{\partial t} \tag{3.35}$$

4

Approach

In this chapter the approach used when taking measurements and how the model parameters are calculated is presented. The valves which the previous presented models are intended for are the ones in a combustion engine, where the dynamic one is intended for low pressure ratios such as when a long route EGR system is used. The system is presented in figure 4.1.

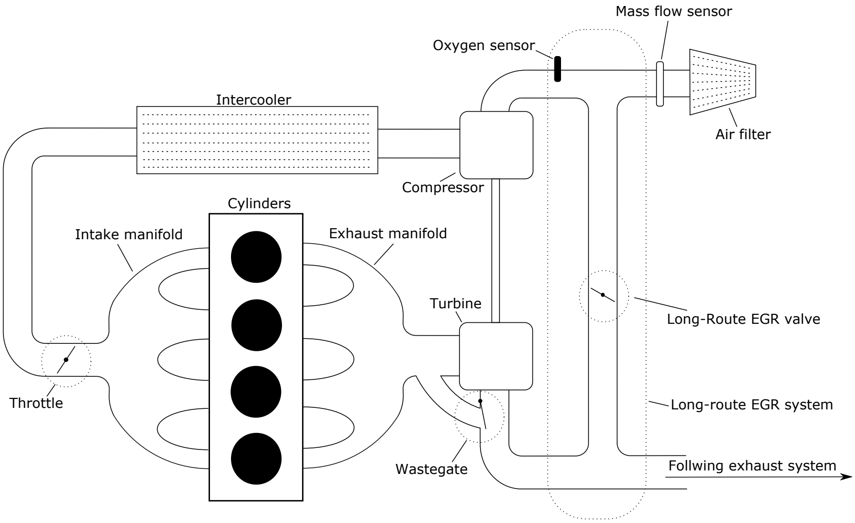
Mass flow sensor
Oxygen sensor
Intercooler
Air filter
Compressor
Cylinders
Intake manifold
Exhaust manifold
Turbine
Long-Route EGR valve
Throttle
Long-route EGR system
Wastegate
Follwing exhaust system

Figure 4.1: *Here a schematic air path system is shown for a turbocharged engine with long route EGR system, long route EGR is shown within the dashed line. The oxygen sensor shown is just an example on how the flow past the long route EGR can be estimated.*

4.1 Steady Compressible Flow

In this section the approach and how the measurements are taken for the steady non-isentropic model is presented.

4.1.1 Approach

To validate the theoretical calculations and formulas in the two sections regarding steady compressible flow in the theory chapter, the approach and some thoughts are described in the following section. The goal is to validate the Ψ-function against real measured data not only theoretically , however the Ψ-function is not a measurable state, some calculations is needed. To start of the isentropical efficiency needs to be determined. This is done by doing measurements on a throttle during steady flow and using the following formula, where all the states are easily measured in the part rightmost, except T_{2a}. The temperature at the throat of the valve cant be measured since it is a very local temperature and after the valve the generated speed causes turbulence and temperature rise. The temperature needs to be determined analytical using ANSYS or the efficiency is to be approximated plotting the Ψ-function and using *lsqcurvefit* to chose the isentropic efficiency that minimizes the error in the model.

$$\eta_N = \frac{V_{2a}^2}{V_{2s}^2} = \frac{T_1 - T_{2a}}{T_1 - T_{2s}} = \frac{T_1 - T_{2a}}{T_1 - T_1\left(\frac{p_2}{p_1}\right)^{\frac{(\gamma-1)}{\gamma}}} \tag{4.1}$$

To determine if the efficiency can be seen as a constant, or if it is pressure ratio dependent, or perhaps throttle angle dependent, measurements need to be done. This is done different pressure ratios, and throttle angles, only then the dependency can be determined. The isentropic efficiency can also be input temperature dependent (T_1), however since it is hard to generate a wide range of input temperatures this will only be investigated for the temperatures which is naturally obtained when making the tests for different pressure ratios, and angles.

The mass flow function is as stated before, here with the addition of an angle, and pressure ratio dependent C_d.

$$\dot{m} = \frac{p_1}{\sqrt{RT_1}} A(\alpha) C_d(\alpha, \Pi) \Psi(\Pi, \eta_N) \tag{4.2}$$

The angle dependant C_d part can be assumed to be absorbed by the $A(\alpha)$ which combined is called $A_{eff}(\alpha)$.

$$\dot{m} = \frac{p_1}{\sqrt{RT_1}} A_{eff}(\alpha) C_d(\Pi) \Psi(\Pi, \eta_N) \tag{4.3}$$

First of assuming that the isentropic efficiency is high enough so that there will be a critical pressure ratio in the Ψ-function. For pressure ratios below the critical pressure ratio the Ψ-function will thus be one, as defined before. Setting the throttle at a fixed position will make the effective area A_{eff} a constant. Making sweeps in the pressure ratio for fixed throttle angle, and normalizing with the values obtained for pressure ratios below the critical pressure ratio, $C_d^*(\Pi)\Psi^*(\Pi,\eta_N)$ can be extracted.

$$\frac{\frac{p_1}{\sqrt{RT_1}}A_{eff}(\alpha)C_d(\Pi)\Psi(\Pi,\eta_N)}{\frac{p_1}{\sqrt{RT_1}}A_{eff}(\alpha)\ \underbrace{C_d(\Pi<\Pi_{crit})\Psi(\Pi<\Pi_{crit},\eta_N)}_{\text{Assumed one for the lowest pressure ratios}}}=\frac{\dot{m}}{\dot{m}(\Pi<\Pi_{crit})}=C_d^*(\Pi)\Psi^*(\Pi,\eta_N) \tag{4.4}$$

In short terms, the mass flow is measured and divided with the mean value of the maximum mass flows, which occurs below the critical pressure ratio, thus the normalized $C_d^*(\Pi)\Psi^*(\Pi,\eta_N)$-function is obtained. The theoretical Ψ-function can now be compared with $C_d^*(\Pi)\Psi^*(\Pi,\eta_N)$ in order to determine if $C_d(\Pi)$ can be neglected, this is done both for isentropic Ψ-function ($\eta_N = 100\%$), and for the non-isentropic Ψ-function which uses isentropic efficiency. This to determine if the Ψ-function taking the efficiency into account can explain the deviations between the isentropic Ψ-function and $C_d^*(\Pi)\Psi^*(\Pi)$, shown in for example (Andersson, 2005) where the $C_d(\Pi)$ can not be neglected. When the Ψ-function have been calculated the effective area function can easily be determined, using some assumed polynomial expression and *lsqcurvefit* to decide the coefficients. The polynomial which is used are proposed in (Eriksson and Nielsen, 2014) and is described in equation (4.5) where a_i are the coefficients which are to be determined.

$$A_{eff} = a_0 + a_1\alpha + a_2\alpha^2 \tag{4.5}$$

4.1.2 Measurements

Since the derived equations assume that the flow is steady, no change with time, and in the intake manifold of an engine there is plenty of pulsations coming from the intake valves the measurements are thus preferable made in a flow bench where there no pulsations are generated. This to ensure that the phenomena which causes the deviation in the theoretical Ψ-function from the measurements in (Andersson, 2005) is not caused by the pulsations. Signals to be measured are temperature and pressure, before and after the throttle, the mass flow past the throttle, and throttle angle. This is done for various fixed throttle angles and for every angle a wide range of pressure ratios. The flow test is carried out at Volvo in their flow bench and a picture of the setup is shown in figure 4.2.

When deciding the $A_{eff}(\alpha)$-function the measurements are done for various throttle angles from the idle opening, to fully open, and for some various pressure ratios that the flow bench can mange to produce when throttle is fully open. Same signals are to be collected in this case.

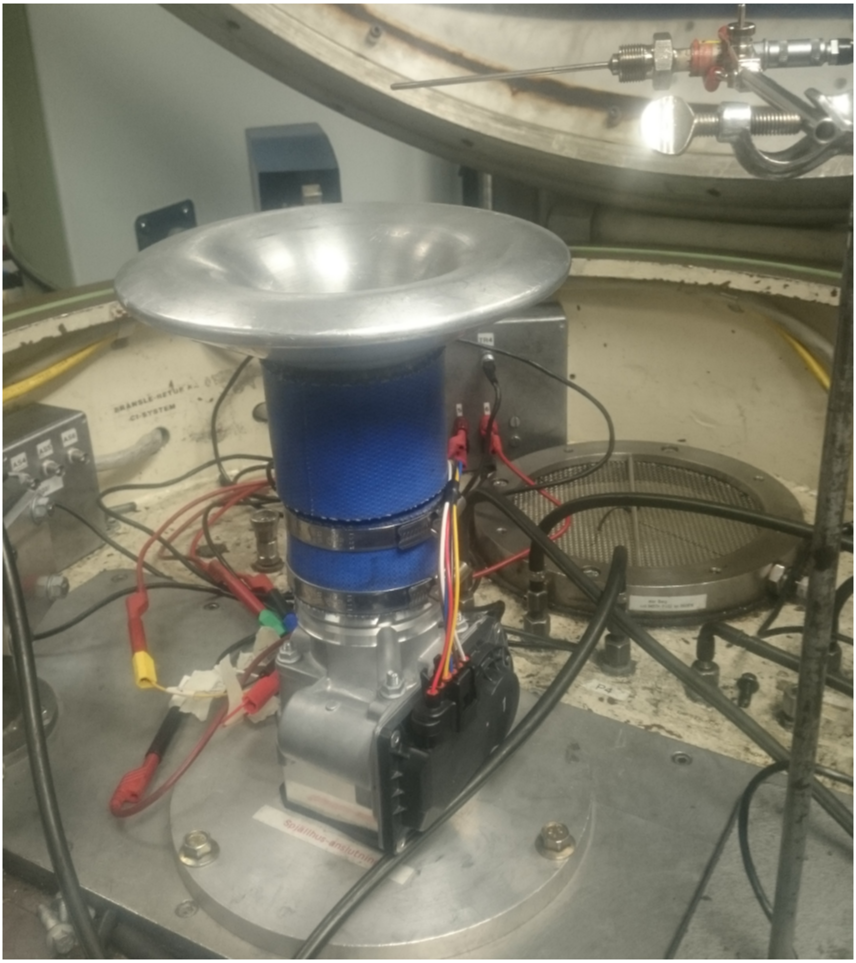

Figure 4.2: Here a standard Volvo throttle housing is mounted with sensors in the flow bench at VCC, a loss free cone is used to reduce inlet turbulence.

4.2 Unsteady Compressible Flow

In this section the theoretical approach by which the dynamic compressible mass flow model parameters can be calculated is presented. Suggestions on how the measurements are to be conducted is also described.

4.2.1 Approach

The approach in which the dynamic compressible flow function is determined is partly the same as for the static equation. The effective area A_{eff} and isentropic efficiency is determined just as for the static function. However the efficiency might be neglected due to the fact that the Ψ-function for pressure ratios close to one is almost the same regardless of the efficiency, and the dynamic function main use is for pressure ratios close to one where the pulsating effects are large and one needs to account for backflow. If one needs a model for a valve which both should work for low pressure ratios where the efficiency needs to be taken into account, and for pressure ratios close to one where the dynamic effects cant be ignored, the previous derived compressible flow equation with regard to efficiency can replace the static part of the dynamic flow equations otherwise the original Ψ-function can be used.

The similarity between the unsteady compressible flow equation and a first order system is striking, the difference is the square of the mass flow term. The square term can however easily be linearized around m_0, here the static term is replaced with ζ and the dynamic term with ϕ.

$$\zeta = \dot{m}^2 + A_{dyn}\phi\frac{d\dot{m}}{dt} \tag{4.6}$$

Variable change:

$$\Delta\dot{m} = \dot{m} - \dot{m}_0 \tag{4.7}$$

And for mass flows close to m_0:

$$\dot{m}^2 \approx \dot{m}_0^2 + 2\dot{m}_0\Delta\dot{m} \tag{4.8}$$

$$\zeta = \dot{m}_0^2 + 2\dot{m}_0\Delta\dot{m} + A_{dyn}\phi\frac{d\Delta\dot{m}}{dt} \tag{4.9}$$

Laplace transforming gives the first order system:

$$\frac{\zeta - \dot{m}_0^2}{2\dot{m}_0 + sA_{dyn}\phi} = \Delta\dot{m} \tag{4.10}$$

The time constant is thus as follows and the A_{dyn} can be determined by making steps in mass flow rate for different plate angles and at different linearized mass flow magnitudes.

$$\frac{A_{dyn}\phi}{2\dot{m}_0} = \tau \tag{4.11}$$

$$A_{dyn} = \frac{2\dot{m}_0\tau}{\phi} \tag{4.12}$$

To determine which variables that affect the dynamic area function further investigations on how a number of parameters, such as mass flow, pressure ratio, temperature and so on, affect the measured values for A_{dyn}. This in order to determine if A_{dyn} can be considered a constant or is dependant on some other parameter and a function can be determined.

4.2.2 Measurements

The data that is to be collected needs to be highly resolved in order to capture the pulsations coming from the filling and emptying of the cylinders. When evaluating the dynamic model on the throttle side a regular mass flow meter can be used, as long as it samples fast enough. However for the long route EGR valve which the dynamic model is intended to be used for the mass flow can not be measured directly. One way to estimate the mass flow over the long route EGR valve is to measure the oxygen level on the intake side of the engine after the mixing point of the fresh air and exhaust gases, see figure 4.1. Defining the percentage of oxygen in a gas as:

$$O_{2\%} = \frac{m_O}{m_{tot}} \tag{4.13}$$

Assuming that the percentage of oxygen in both fresh air and exhaust gas is known the precentage of oxygen after the mixing point can be described as:

$$O_{2\%} = \frac{O_{2\%air}\dot{m}_{air} + O_{2\%exhaust}\dot{m}_{EGR}}{\dot{m}_{air} + \dot{m}_{EGR}} \tag{4.14}$$

Thus the mass flow over the EGR valve can be described using a mass flow sensor and an oxygen sensor.

$$\dot{m}_{EGR} = \dot{m}_{air}\frac{O_{2\%air} - O_{2\%}}{O_{2\%} - O_{2\%EGR}} \tag{4.15}$$

This approach is however problematic since oxygen sensors is not fast enough to measure the pulsations which occurs twice per engine revolution in the intake manifold. A high resolved air mass flow sensor can be used instead and the dynamic model thus have to be evaluated on the throttle instead of the EGR valve.

5

Results

Here the results of this master's thesis is presented. For example the measured data both from an engine and a flow bench against standard and extended model is shown. The simulation results from both ANSYS and SIMULINK is also presented.

5.1 Fixed Throttle Position

In order to eliminate the area dependant factor when calculating the Ψ-function measurements are made for fixed throttle positions, thus the effective area can be seen as a constant and eliminated. Measurements are made for three different throttle angles, however for the throttle angle at 5 degrees only a very small range of pressure ratios was possible to archive due to the limitations in the engines working range. These measurements are made on an engine thus the intake pulsations is present. One can clearly see the deviation between the measured and theoretical values in figure 5.1, just as in (Andersson, 2005).

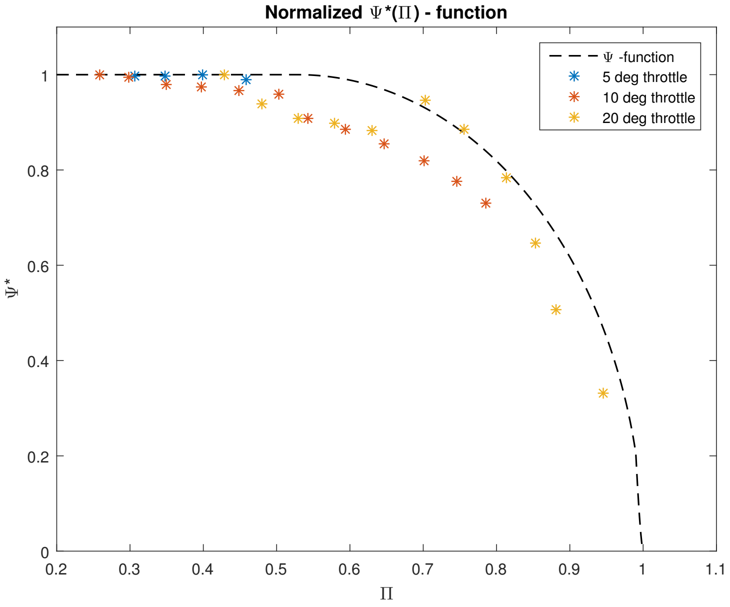

Figure 5.1: *The Simulation model used to calculate the normalized* Ψ*-values for different pressure ratios with the effect of intake manifold pulsations.*

5.2 Normal and Extended Ψ-function

Using data where the pressure before and after the throttle, temperature before the throttle, mass flow past the throttle, and throttle angle are measured during stationary conditions makes it possible to evaluate the Ψ-function. Furthermore the isentropic flow equation is used and compared with the non isentropic flow equation in order to determine if an improvement is achieved.

5.2.1 Engine Measurements

These measurements are made on an engine, thus the pulsations are present, and the deviation in the Ψ-function can not definitely be explained by the efficiency, it can also be the pulsations effecting the flow. In figure 5.2 the isentropic flow equation is used, and in figure 5.3 the non-isentropic flow equation is used and the optimal efficiency is determined using *lsqcurvefit*. In order to eliminate the effective area term from the model the effective area is modeled and then substituted in order to obtain the Ψ-function. In figure 5.4 the difference between the fit of the normal and extended Ψ-function is shown along with the calculated Ψ-values from the data.

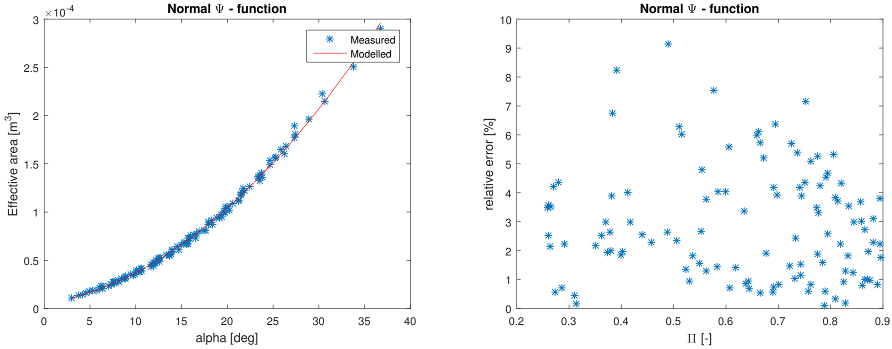

(a) Measured and modelled effective area when the isentropic Ψ-function is used.

(b) Relative effective area error when the isentropic Ψ-function is used.

Figure 5.2: *Effective area model when the isentropic Ψ-function is used. The mean relative error is in this case 2.89%*

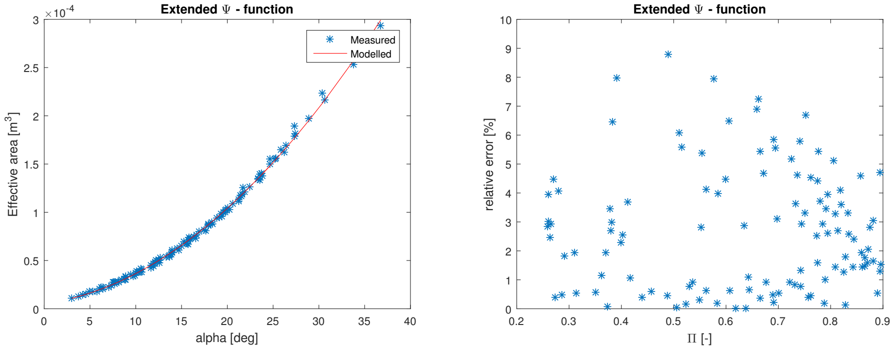

(a) Measured and modelled effective area when the non-isentropic Ψ-function is used.

(b) Relative effective area error when the non-isentropic Ψ-function is used.

Figure 5.3: *Effective area model when the non-isentropic Ψ-function is used, the efficiency which minimizes the relative error is 96.5%. The mean relative error is in this case 2.69% which is a 7% decrease in relative error.*

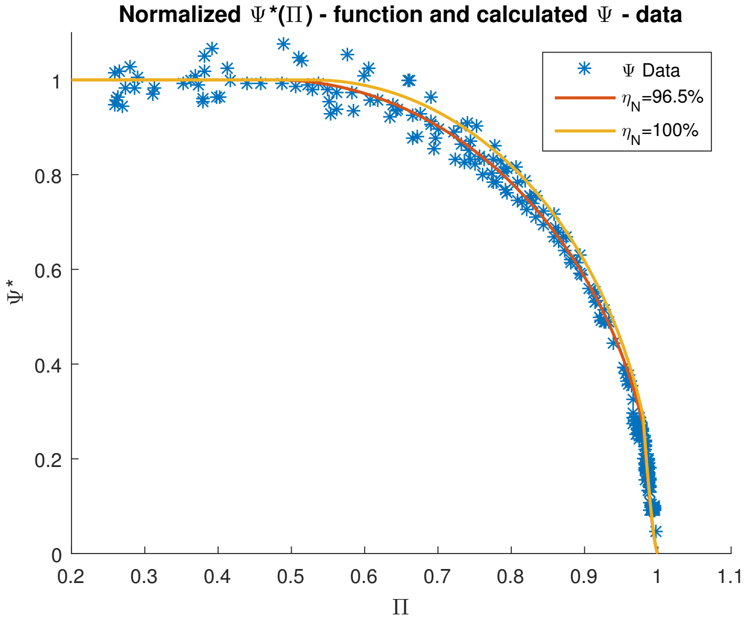

Figure 5.4: *The normalized* Ψ*-data points is here shown together with both the standard* 100% *isentropic efficiency equation and with* 96.5% *efficiency, which is obtained using* lsqcurvefit.

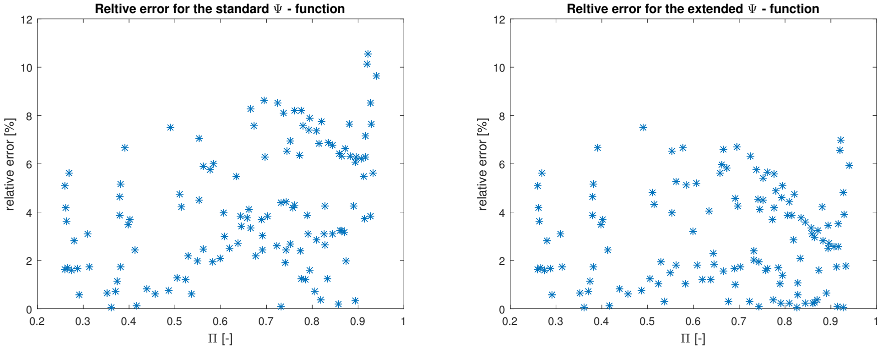

*(**a**) Relative error when the standard* Ψ*-function is used, the mean relative error is here 4.16 %.*

*(**b**) Relative error when the extended* Ψ*-function is used, the mean relative error is here 2.92 %.*

Figure 5.5: *Pressure ratios above 0.95 is removed due to the linear region in the model which have a big relative error and thus only makes it harder to compare the improvement in the model. The total improvement in relative error is over 30% for the extended model.*

5.2.2 Flow Bench Measurements

These measurements are made with a flow bench, thus pulsations are not present, and the deviation in the Ψ-function can with these results with certainty exclude the pulsations as the deviating factor.

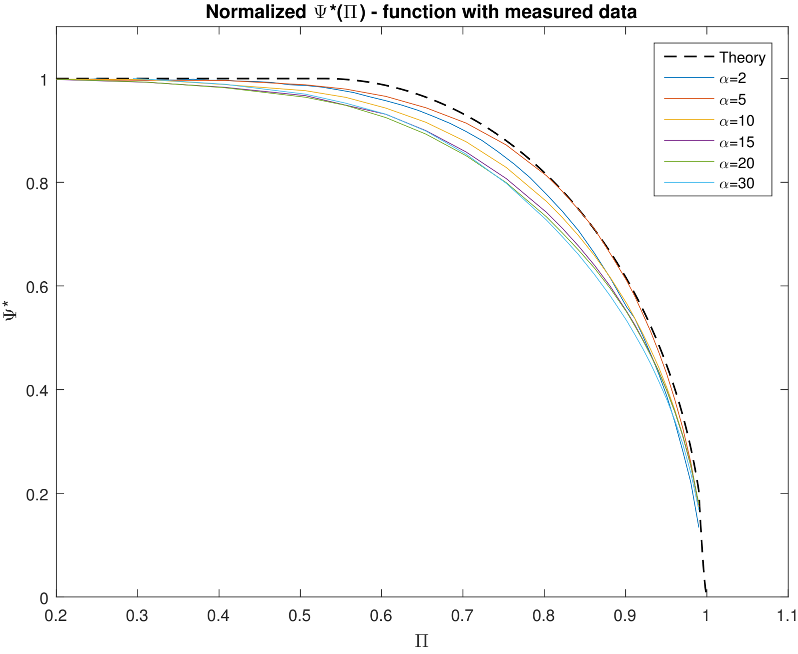

Figure 5.6: *The isentropic normalized Ψ-function is here shown together with the data collected in the flow bench for various throttle angles. One can see that the efficiency is varying with the throttle angle and the figure indices that a smaller opening have higher efficiency.*

The data collected in the flow bench is used to calculate the efficiency for every fixed area opening using *lsqcurvefit*, the result is shown in figure 5.7. The error between the measured values and the non-isentropic Ψ-function when the estimated efficiency is used is very small, more details of the relative error is shown in figure 5.8. Using a non-pressure dependant efficiency can be motivated by the small differences in relative error over the Π-range. Also the area dependant effect on the isentropic efficiency can perhaps be neglected, the only big deviation in efficiency is for a throttle opening of 5 degrees.

The Reynold's number can be calculated using equation (5.1). The results when calculating the Reynold's number can be seen in figure 5.9. For a fluid flowing in circular pipe the critical Reynold's number where the flow is shifting from laminar to turbulent is said to be around $2000 < Re < 4000$ and if there is some obstacle or a rough surface in the tube turbulent flow will evolve much faster,

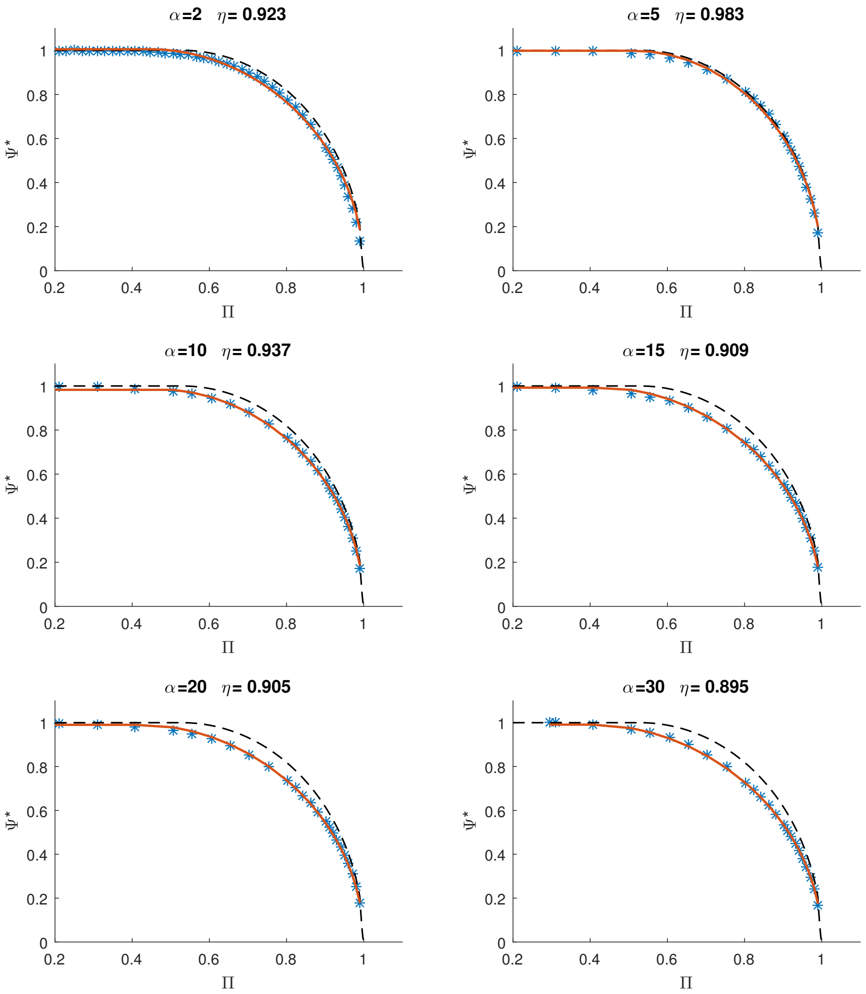

Figure 5.7: *The isentropic Ψ-function is the dashed line, the measured values from the flow bench is the blue line, and the red line is the non-isentropic Ψ-function when the efficiency is estimated using* lsqcurvefit*.*

(Karl Storck, 2012). The flow is according to the calculated Reynold's number fully developed turbulent in all the cases.

$$Re = \frac{LU}{v} = \frac{d_h \frac{\dot{m}}{\rho A}}{v} = \frac{\frac{4\dot{m}}{O\rho}}{v} = \frac{\frac{4\dot{m}RT}{Op_2}}{v} \tag{5.1}$$

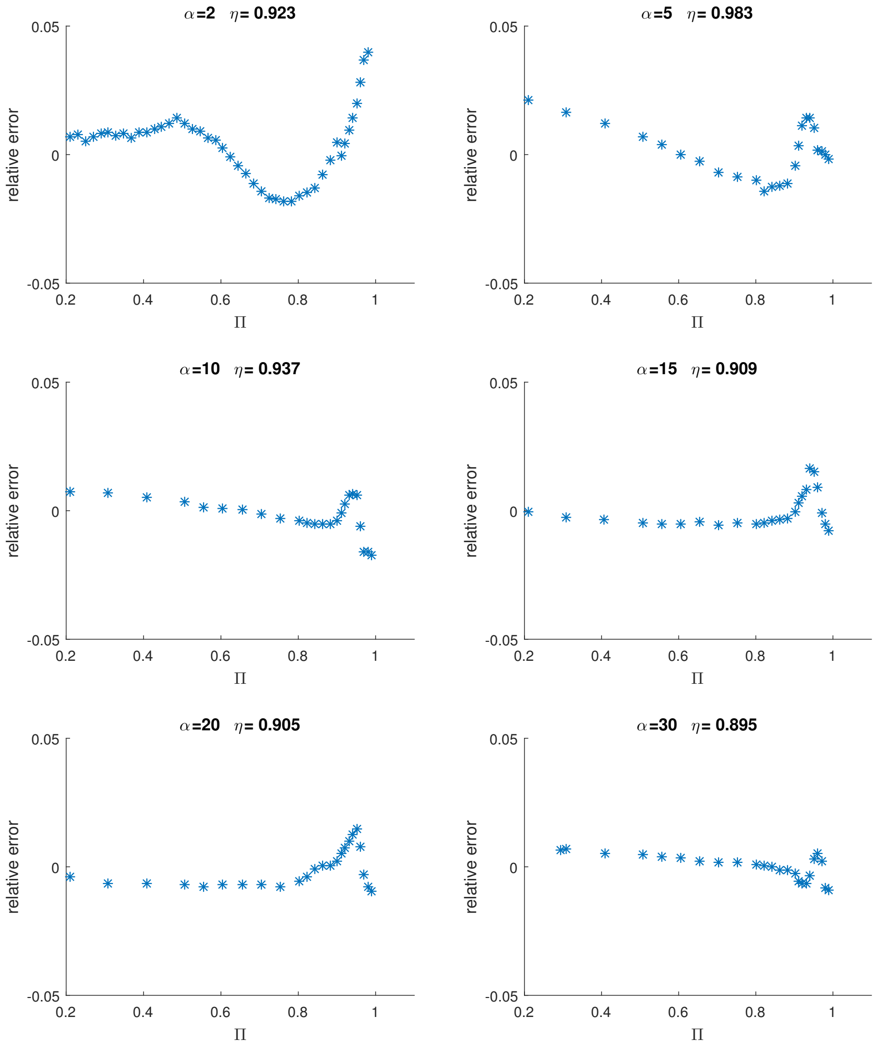

__Figure 5.8:__ The relative error is here shown for the different throttle angles, there is no apparent tendencies except that the relative error is a bit higher for pressure ratios close to one, this since the function here his closer to zero which leads to higher relative error even if the absolute error is the same or even smaller.

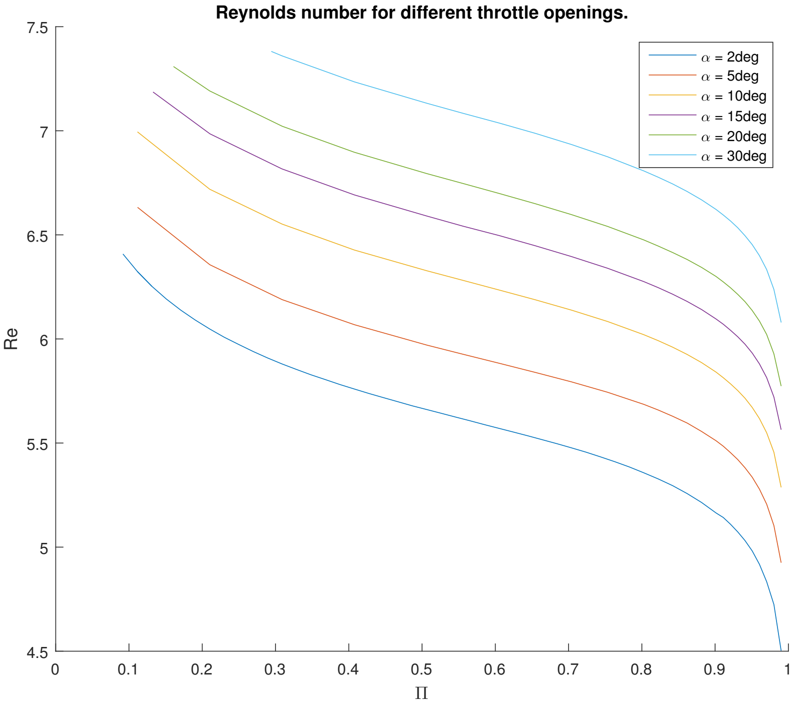

Figure 5.9: *Here the Reynold's number is shown for the different throttle openings and over the pressure ratio, there is in all cases fully developed turbulent flow. The Reynold's number is here calculated at the throat of the valve assuming the valve opening is shaped as a two dimensional crescent.*

5.3 Pulsating Pressure Ratio

The effects of a mean pressure ratio when calculating the momentarily mass flow is described in the theory chapter and is here evaluated. First of is to determine the shape and size of the pressure pulsations in the intake manifold, this is done by measuring with a fast enough pressure sensor for three different output torques, 30 Nm, 80 Nm, and 280 Nm , pressure pulsations shown in figure 5.11. The mean value of each signal is then removed in order to obtain only the shape and height of the pulsations. A simulation system is then built in SIMULINK, see figure 5.10 where the different intake pressure is sent to the model from the workspace of MATLAB and the pressure pulsations are added, this is done for pressure ratios of 0.2 to 1. The result of the simulation model is shown in figure 5.12, and the effects of the pulsations is as seen negligible. The use of a mean value pressure ratio is not enough to explain the distortion of the Ψ-function. However close to pressure ratio one where the amplitude of the pulsations is enough to drive the flow in the opposite direction the fit is bad due to the fact that the used model cant handle back flow.

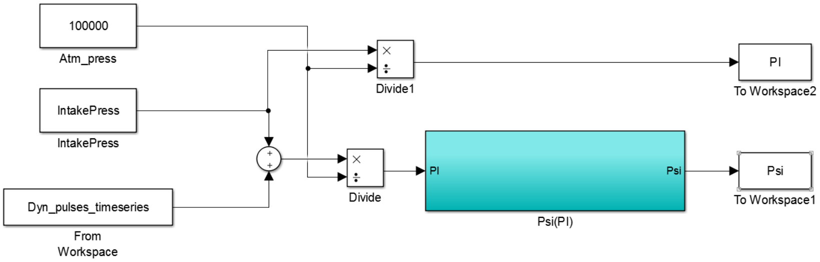
100000
Atm_press
IntakePress
IntakePress
Dyn_pulses_timeseries
From
Workspace
+
+
×
÷
Divide1
×
÷
Divide
PI
Psi
Psi(PI)
PI
To Workspace2
Psi
To Workspace1

Figure 5.10: *The Simulation model used to calculate the normalized Ψ-values for different pressure ratios with the effect of intake manifold pulsations.*

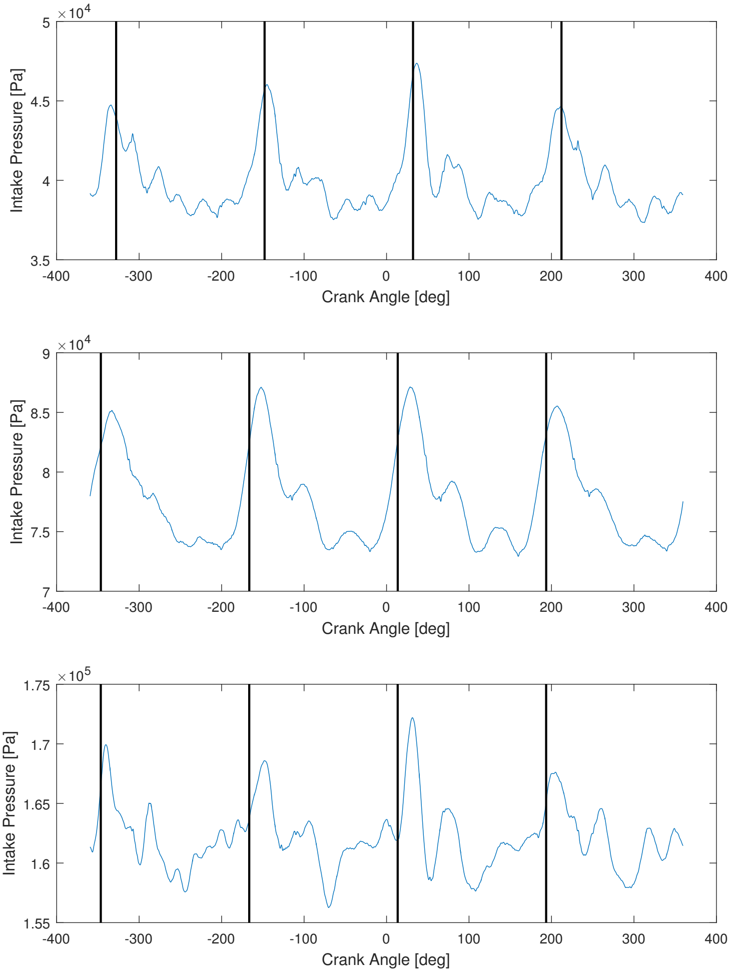

Figure 5.11: *Intake manifold pressure pulsations for three different engine loads, first is* 30 *Nm where the amplitude is* 10 *kPa, second* 80 *Nm where the amplitude is* 14 *kPa, and last* 280 *Nm where the amplitude is* 16 *kPa. The vertical lines shows where the intake valve closes for each cylinder.*

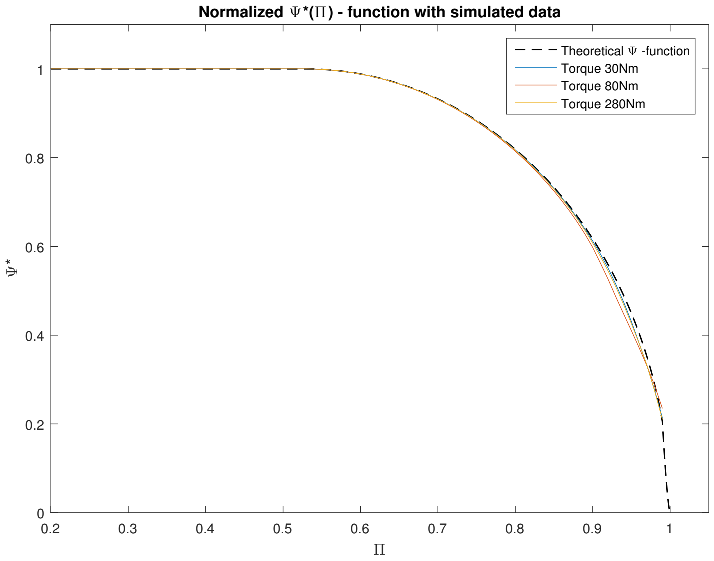

Figure 5.12: *The theoretical Ψ-function along with the calculated Ψ-function for the three different engine load pressure pulsations. The deviation from the theory close to pressure ratio one is due to the fact that the pulsations causes pressure ratio to go above one which leads to back flow which is not taken into account in the model. The deviation from theory due too pulsations is to small and can not explain the quite large deviation shown in (Andersson, 2005)*

5.4 Throttle Valve ANSYS Analysis

A throttle valve is modeled in two dimensions with a pipe diameter of 60 mm and a plate angle of 20 degrees. The mesh is done fairly large upstream and downstream of the openings to reduce calculation time, however around the openings very small elements are used to obtain high accuracy. The calculations are done for two different pressure ratios which are shown in figure 5.13. The corners of the valve body is rounded to remove sharp edges which requires extremely fine mesh size in order to keep the simulation converging.

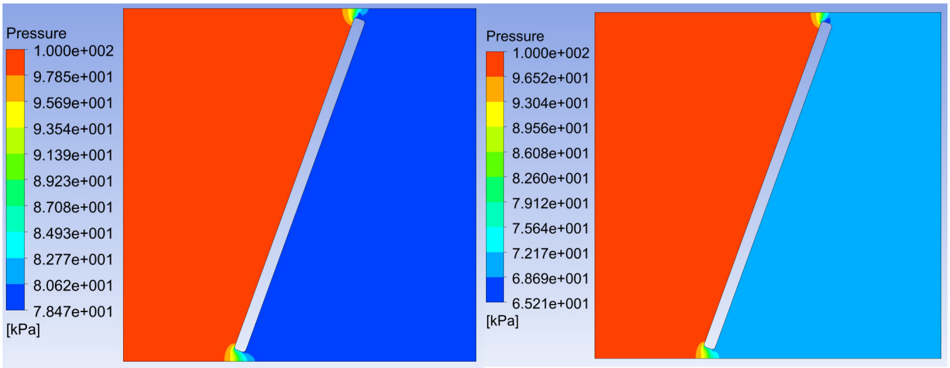

(a) Pressure contours over the throttle valve when pressure ratio is 0.8.

(b) Pressure contours over the throttle valve when pressure ratio is 0.7.

Figure 5.13: *The static pressure is shown over the throttle valve.*

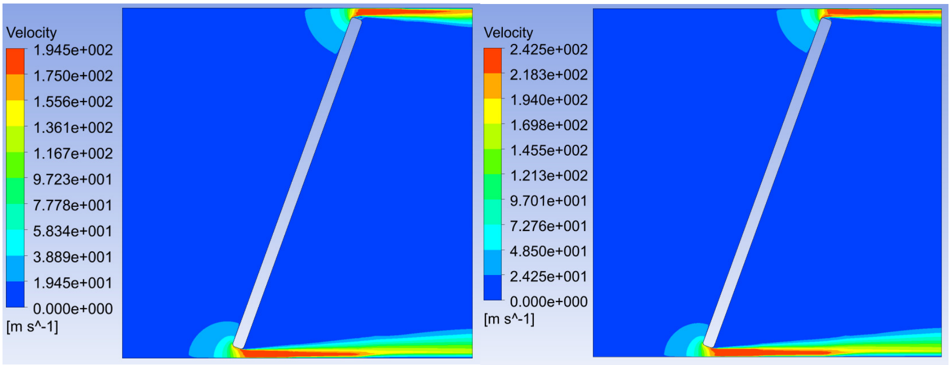

(a) velocity magnitude over the throttle valve when pressure ratio is 0.8.

(b) Velocity magnitude over the throttle valve when pressure ratio is 0.7.

Figure 5.14: *The velocity magnitude is shown over the throttle valve.*

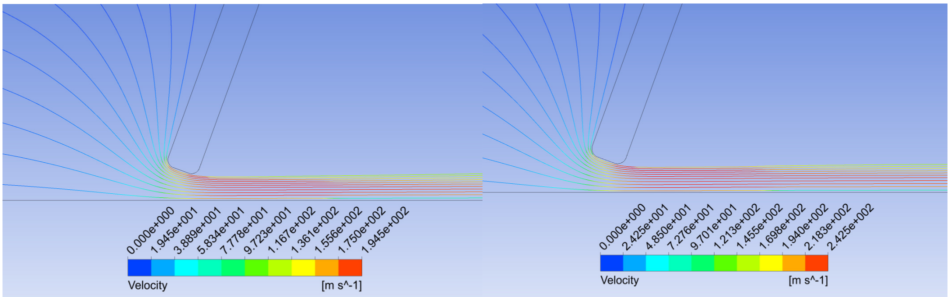

(a) *The streamline function with velocity magnitude over the lower opening in the throttle valve when pressure ratio is* 0.8.

(b) *The streamline function with velocity magnitude over the lower opening in the throttle valve when pressure ratio is* 0.7.

Figure 5.15: *The shape of the streamlines are very similar between the two pressure ratios.*

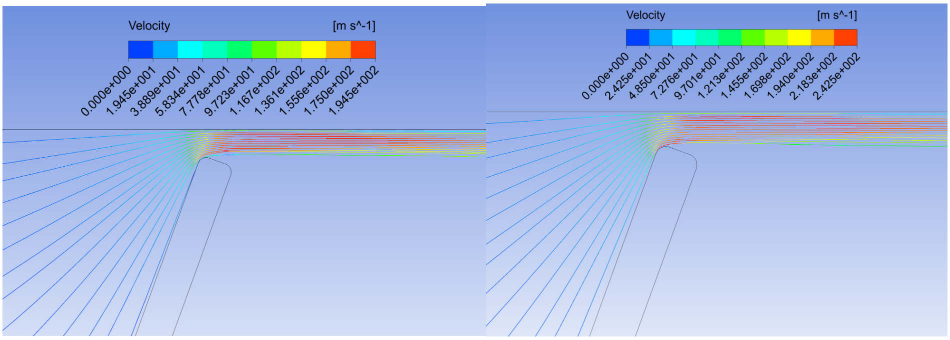

(a) *The streamline function with velocity magnitude over the upper opening in the throttle valve when pressure ratio is* 0.8.

(b) *The streamline function with velocity magnitude over the upper opening in the throttle valve when pressure ratio is* 0.7.

Figure 5.16: *The shape of the streamlines are very similar between the two pressure ratios.*

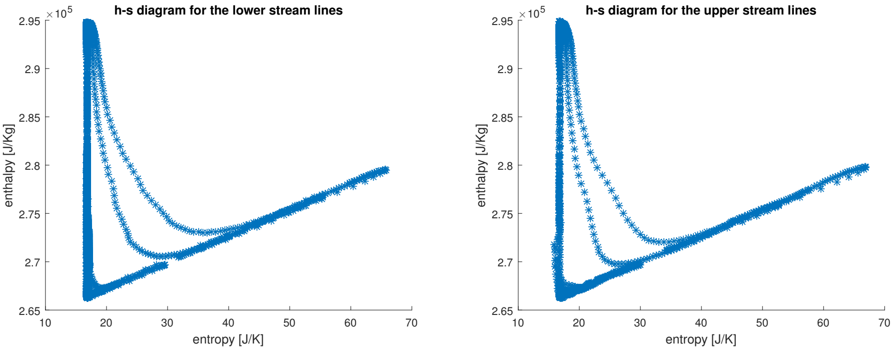

*(**a**) The throttling process for the lower opening in the valve, this for a pressure ratio of* 0.7*.*

*(**b**) The throttling process for the upper opening in the valve, this for a pressure ratio of* 0.7*.*

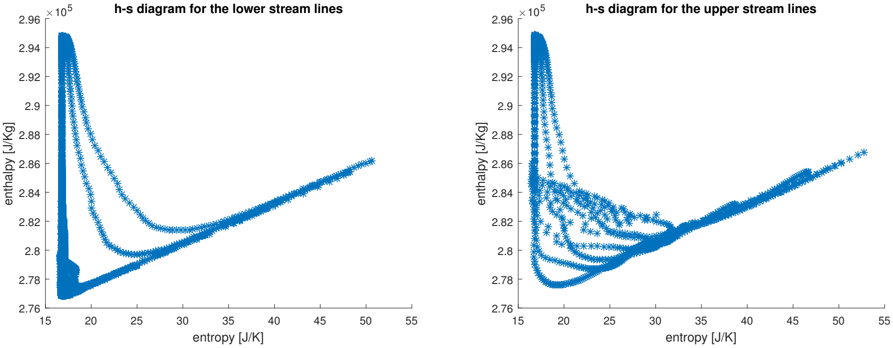

*(**c**) The throttling process for the lower opening in the valve, this for a pressure ratio of* 0.8*.*

*(**d**) The throttling process for the upper opening in the valve, this for a pressure ratio of* 0.8*. Here the flow simulated does not seem to be fully developed.*

***Figure 5.17:** Enthalpy and entropy for the throttling process for the lower and upper streamlines. The process seems to be ideal, this might be since the calculations are done with a model for turbulence which simplified the flow with a turbulent flow model.*

5.5 Dynamic Compressible Flow

A regular mas flow meter measures the air mass flow through the pipe with the help of a platinum wire. A current is sent through the wire, the more mass flow the more the wire will be cooled which leads to lower resistance and the other way around for lower mass flows. The mass flow can thus be measured after the sensor has been calibrated towards a known flow in a flow bench. The dynamic measurements is carried out in the engine-lab at ISY with one millisecond sampling of the new mass flow sensor which uses a thin film to measure the varying resistance instead of a platinum wire as before. The film reacts much faster to changes than the wire due to the greater area to mass ratio which cools or heats the film faster then the wire. The raw measured signals for the mass flow can be seen in figure 5.18 and the related intake manifold pressure in figure 5.19. The measured boost pressure (pressure before the throttle) can be considered constant since it only oscillates with the resolution of the digital pressure sensor, 0.08 kPa.

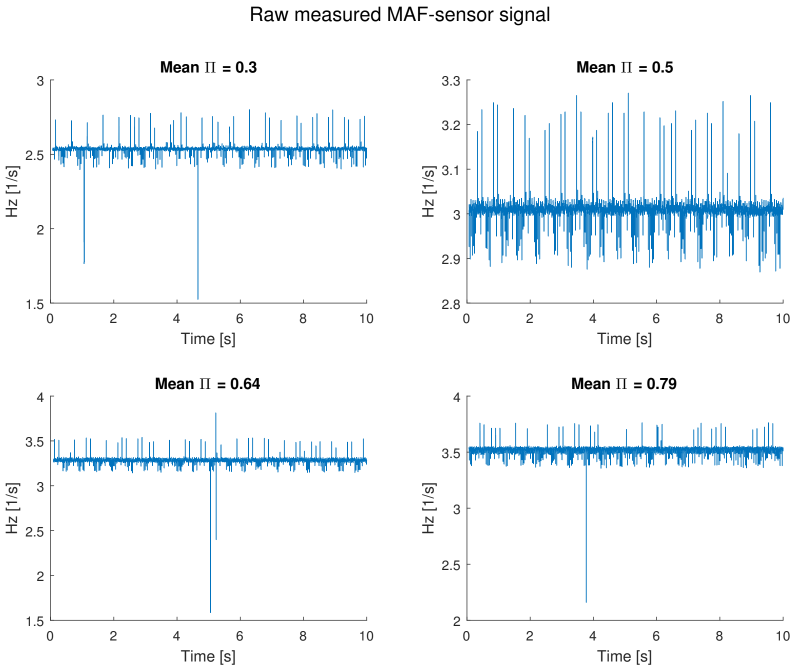

Figure 5.18: *The measured air mass flow signal for four different loads and thus pressure ratios, the frequency needs to be converted to mass flow with the help of the calibration line for this particular sensor. The sudden spikes in the data is probably measurement errors due to bad connections in the wiring.*

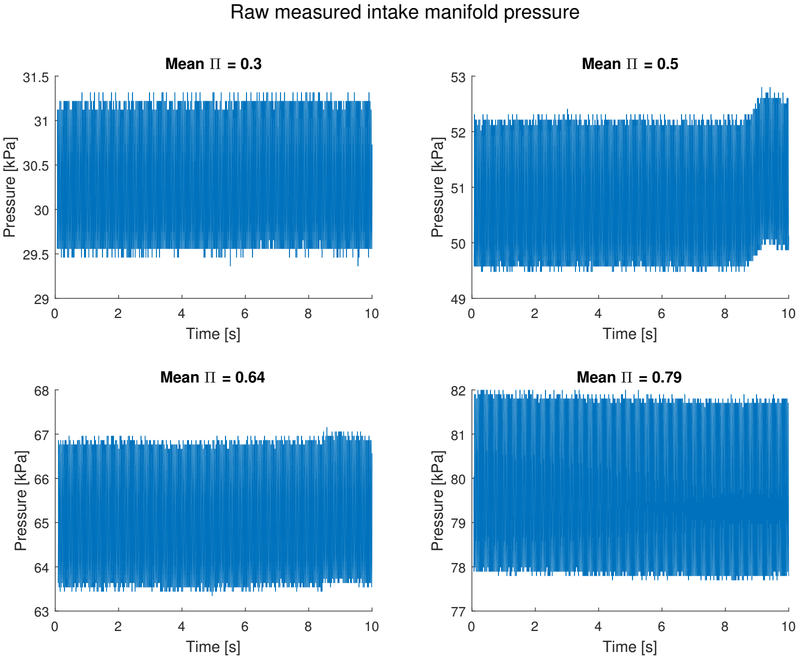

Figure 5.19: *Here the intake manifold pressure for the four different cases can be seen, in the case of pressure ratio* 0.5 *some load change happens at the end. Here the data is cleaner and needs no pre-filtering as in the mass flow case.*

The data from the mass flow sensor is pre-filtered by replacing the values that deviate too much from the previous values in the time series with the previous value, this removes the sudden spikes that can be seen in the raw air mass flow sensor signal. Furthermore both intake manifold pressure signal and the mass flow signal is filtered with a *butterworth* filter and the *filtfilt* function in MATLAB, which is a no phase shifting filter. After filtering the frequency from the mass flow sensor, the frequency is converted to actual mass flow air in grams per second using the given calibration line supplied by VCC, shown in figure 5.20. The filtered and the raw signal for the mass flow can be seen in figure 5.21 which is zoomed so it is possible to see the difference, where the zoom position is randomly chosen. The same case for the pressure in the intake manifold can be seen in figure 5.22.

Furthermore the pressure signal is applied to the static non-isentropic compressible flow equation with an isentropic efficiency of 95%, the effective area function is calculated from data taken in the flow bench see figure 5.23. The resulting modelled mass flow is then compared to the measured and the result can be seen in figure 5.24, the mean flow was corrected by a very small portion just

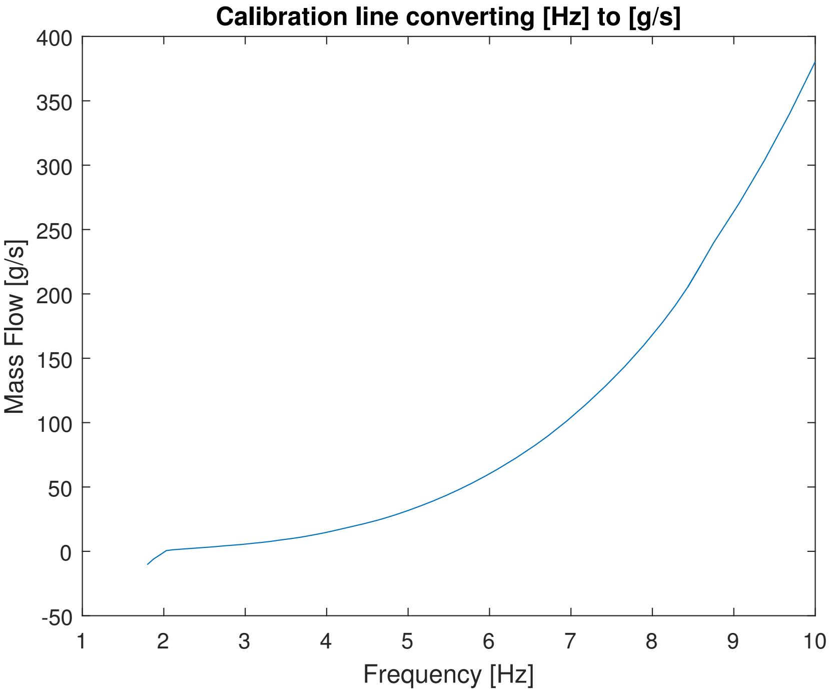

Figure 5.20: *The calibration line converting the measured frequency to air mass flow in grams per second, this particular mass flow meter can even handle back flows thus presenting a negative value.*

so that the mean flow of both signals is at the same level which makes it easier to compare. The phase difference between the model and the measured values is due to the distance from measured pressure to measured mass flow which causes a time delay. However in order to implement the dynamic flow equation to predict the instantaneous flow past the throttle the measurements should have been done without any turbo or intercooler which disturbs the flow. A spectral analysis is made and the result is shown in figure 5.25

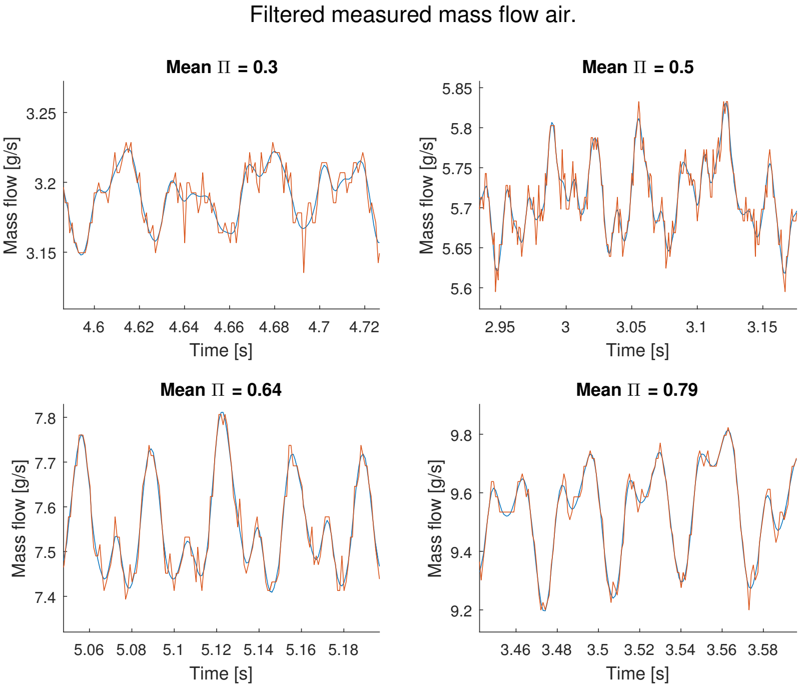

Figure 5.21: *Here the filtered mass flow signal can be seen together with the raw signal, the blue line is the filtered signal and the red is the raw data. After pre-filtering and filtering the data is converted from frequency to mass flow.*

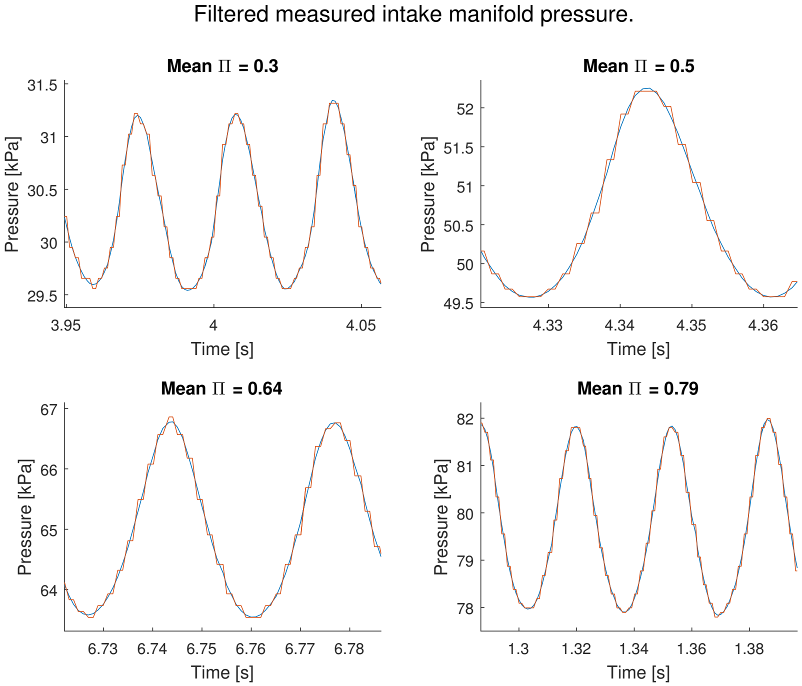

Figure 5.22: *Here the filtered intake manifold pressure signal can be seen together with the raw signal, the blue line is the filtered signal and the red is the raw data. The resolution of the digital pressure sensor can also be seen here as the steps in the red line.*

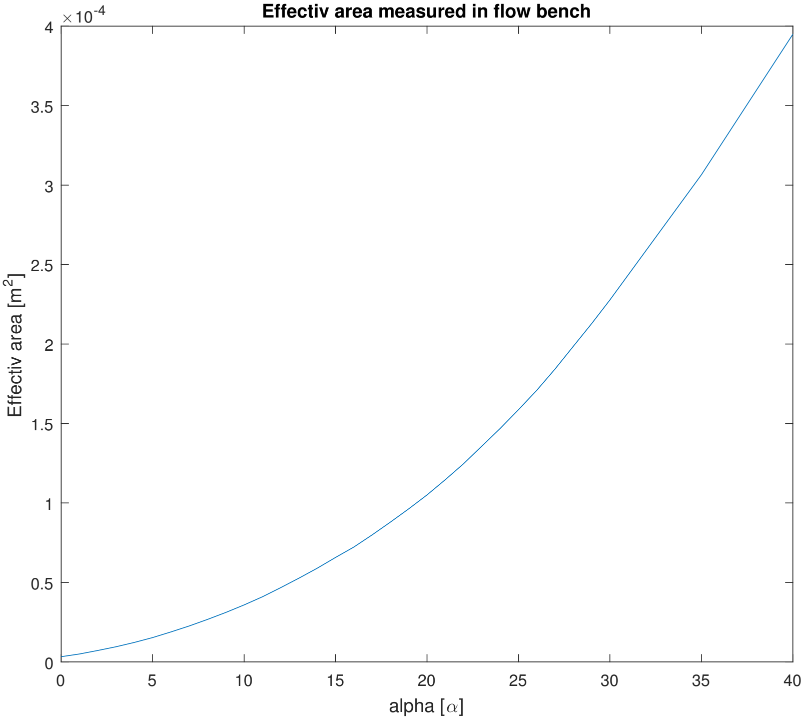

Figure 5.23: *Here is the measured effective area shown, this line is used when calculating the flow from the pulsating intake manifold pressure.*

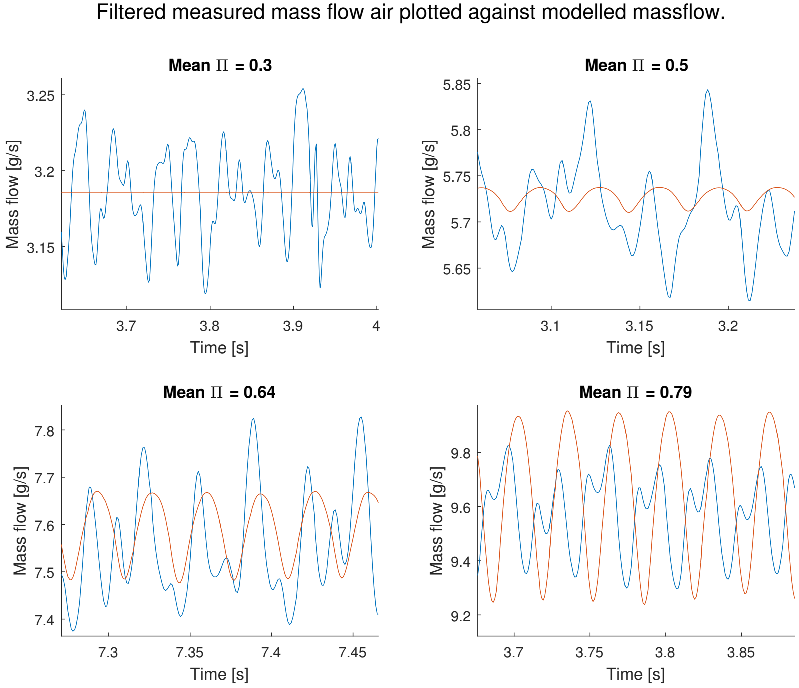

Figure 5.24: *Here the measured mass flow signal, blue line, together with the modelled mass flow, red line, is shown. When pressure ratio is below the critical pressure ratio the model indicates a constant flow, the pulsations for the lowest pressure ratio is thus induced by the compressor and the intercooler volume. It is in this case impossible to distinguish the mass flow pulsations coming from the flow past the throttle or the pulsations induced from the speed of the turbo.*

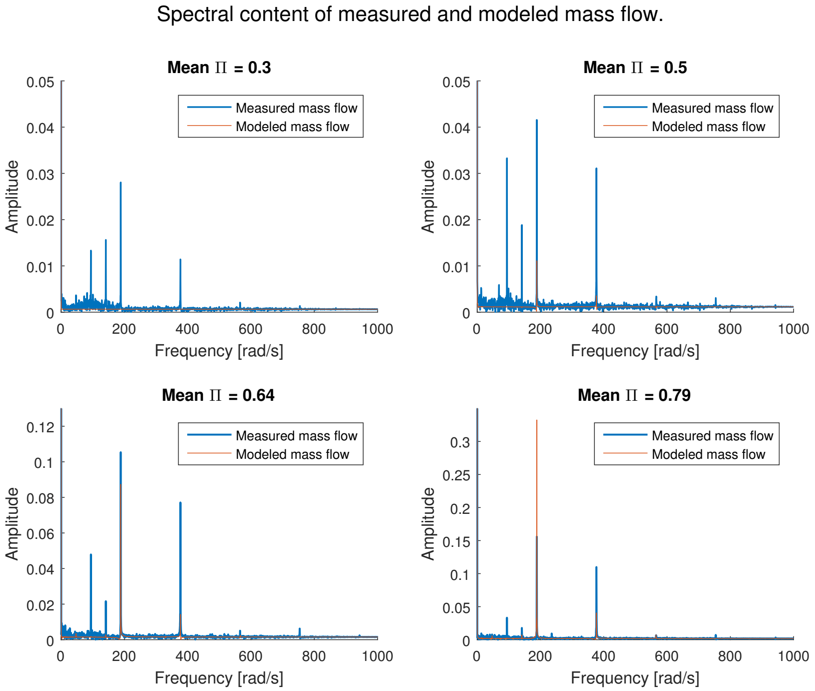

Figure 5.25: *Here a fourier transfrom is made for the different signals in order to see the spectral content of each signal. The engine was running at 950 rpm which can clearly be seen as the main frequency at almost 200 rad/sec. Each valve opens every second revolution, thus 2 valves open per revolution in a four cylinder engine, which is 200 rad/sec at 950 rpm. There is also a lower peek at 100 rad/sec which is the opening of one valve. Overtones of the base frequency can also be seen, some of the pulsations in the measured signals comes from the intake manifold and some from the exhaust pulses driving the turbo.*

6

Conclusion

In this chapter the conclusion and summary of this master's thesis is presented, along with some suggestions for future work.

6.1 Summary

This master's thesis have focused on the standard isentropic adiabatic compressible flow equation for a nozzle and evaluated how well the assumptions made when deriving the equation fits the conditions for a throttle in a combustion engine. Already in (Andersson, 2005) and among others, measurements shows that some of the assumptions made when deriving the standard compressible equation might have been too much of a simplification. Such measurements have been done in this master's thesis as well and the same effect has been found. Here follows a short list of the assumptions which were investigated.

- The first assumption which was investigated was the usage of a mean pressure ratio when calculating the mass flow. Typical intake manifold pulsations were measured with fast sampling sensors and the resulting pressure ratio was inserted into a SIMULINK model which calculated the mean mass flow and presented a Ψ-function. This was done for three different engine loads, thus three different amplitudes of the pulsations. The result shows that for typical intake manifold pulsations the resulting Ψ-function do not deviate as much as shown in (Andersson, 2005). The deviation is also largest at pressure ratios close to one which is the opposite as the measurements shows in (Andersson, 2005), thus the assumption that the flow is steady is good enough, at least for the throttle. However where pressure ratio is close to one and the pulsations are larger this assumption leads to modeling errors, such as for the long route EGR valve.

- The second assumption is that the flow is both adiabatic and isentropic, adiabatic means no heat exchange with the surrounding, and isentropic means constant entropy. Both these assumptions correlates to the internal energy of the gas and are therefore lumped into one assumption, this since it needs extensive tests to show where the energy is coming from if it exchanges energy with the surrounding or energy is generated within. Where the energy is coming from is not that interesting, the interesting part is how it affects the flow. Instead of this assumption an efficiency term is introduced, which can simplified be described as the amount of useful enthalpy drop divided by the ideal enthalpy drop over the valve. A new equation is derived with this in mind, in appendix B, the results are promising and the deviation in the ideal Ψ-function can be explained by this. The ANSYS analysis indicates a generation of entropy in the streamlines close to the wall, however no generation of entropy is seen in the other streamlines which does not go along with the results from the equation and the good fit to the data. This can be explained by the simplification ANSYS does when calculating turbulent flow, due to lack in computational power and knowledge about ANSYS fluent the simulation were not complex enough to capture the generation of entropy. However the model fits well to the data taken in a flow bench and the efficiency term is around 92.5% which is in line with what is stated in (Çengel et al., 2012).

- The third assumption is that the effective area function $A_{eff}(\alpha)$ only depends on the throttle plate angle α and is not dependant on the pressure ratio $A_{eff}(\alpha, \Pi)$. Due to the difficulty in pinpointing where in the model the deviation is coming from, if it is the Ψ-function or the area function this has only been investigated by looking at the streamlines in the ANSYS simulation. The streamlines in the ANSYS analysis does not indicate that the streamlines are contracting at higher pressure ratios, however here is a lot of uncertainties due to the lack of computational power once again which could not simulate pressure ratios below 0.7. Due to the limitations and large uncertainties in this method it is not investigated further when the second assumption seems to be the problem in the model.

The improved model which does not assume adiabatic and isentropic flow have improved the modeling accuracy by decreasing the relative error for both the effective area function by 7% and for the Ψ-function by 32%. The data used here is 236 different stationary operating points for the Volvo engine in the engine-lab, a so called engine map.

Furthermore this master's thesis introduces a dynamic flow model which utilizes the 1-D momentum equation to add an extra dynamic term to the regular mass flow model. The dynamic equation handles back flow by shifting the sign of the flow and replacing pressure and temperature with the upstream pressure and temperature. The model is intended for places where the pressure ratio is close to one and there is large pulsations, meaning the pulsating effect is not negligible here. This occurs in for example the exhaust and more specific the long route EGR valve. However due to the harsh conditions in the exhaust and not being able to measure the flow over such a valve the measurements where taken on a throttle. The pulsations are not as big here and there is an intercooler and a turbo influencing the measurements in-between of the throttle and the fast sampling MAF-sensor the connection between the dynamic flow model and the measured data was never made. The spectrum of the signals where investigated but in order to implement and finding the terms in the dynamic model more work is needed.

6.2 Future Work

The time spent on this thesis has unfortunate come to an end, however this intriguing subject leaves if possible more to think about now than before the work started. The two main working directions in the future is proposed here.

6.2.1 Ψ-function

In order to be certain that the reason for the deviation in the standard Ψ-function is the generation of entropy further analysis is needed. This can preferable be done by someone who have more knowledge in ANSYS fluent and have access to a super computer. This will show if there is a generation of entropy or if it is some other effect, however this might not be of interest since the new model correlates well with the data. Investigations if it is sufficient to assume the efficiency to be seen as a constant or if there is a need for an efficiency function, some work have been done in this thesis on this subject but more is perhaps needed.

6.2.2 Dynamic Flow Model

The dynamic flow model needs to be investigated further, for example how the coefficients should be extracted from measurements and how the measurements should be done, both practical and in theory in order to easily obtain the coefficients needed for an implementation of the model. Another solution is also to model the dynamics of the system between measuring point and the throttle valve, which makes it possible to estimate the instantaneous flow past the throttle. When this is done the model can be evaluated. Measurements are preferable done under such conditions for which the model is intended, as in a long route EGR system of a combustion engine. However the model is hopefully a good starting point when modeling the pulsating and back flowing behaviour of valves such as the long route EGR.

Appendix

A

Calculations for Isentropic Compressible Flow

Some ideal gas relations:

$$\gamma = \frac{c_p}{c_v} \tag{A.1}$$

$$c_p = c_v + R \tag{A.2}$$

$$c = \sqrt{\gamma R T} \tag{A.3}$$

$$\rho = \frac{p}{RT} \tag{A.4}$$

Calculations for equations (3.3), **and** (3.5) **to** (3.6)**.**

Proof:

$$V = M\sqrt{\gamma R T} \tag{A.5}$$

$$T_1 = T_2 + \frac{(M\sqrt{\gamma R T_2})^2}{2c_p} \tag{A.6}$$

$$\frac{T_1}{T_2} = 1 + \frac{M^2 \gamma R}{2c_p} \tag{A.7}$$

$$\frac{T_1}{T_2} = 1 + \frac{M^2}{2}\frac{c_p(c_p - c_v)}{c_v c_p} \tag{A.8}$$

$$\frac{T_1}{T_2} = 1 + \frac{M^2}{2}(\gamma - 1) \tag{A.9}$$

$$\frac{T_1}{T_2} = 1 + \frac{\gamma - 1}{2} M^2 \tag{A.10}$$

□

Calculations for equations (3.3)**,** (3.4)**, and** (3.5) **to** (3.7)**.**

Proof:

$$\frac{T_1}{T_2} = 1 + \frac{\gamma - 1}{2} M^2 \tag{A.11}$$

$$\frac{T_2}{T_1} = \left(\frac{p_2}{p_1}\right)^{\frac{(\gamma-1)}{\gamma}} \tag{A.12}$$

$$\left(1 + \frac{\gamma - 1}{2} M^2\right)^{-1} = \left(\frac{p_2}{p_1}\right)^{\frac{(\gamma-1)}{\gamma}} \tag{A.13}$$

$$\left(1 + \frac{\gamma - 1}{2} M^2\right)^{-1} \left(\frac{p_1}{p_2}\right)^{\frac{(\gamma-1)}{\gamma}} = 1 \tag{A.14}$$

$$\left(\frac{p_1}{p_2}\right)^{\frac{(\gamma-1)}{\gamma}} = \left(1 + \frac{\gamma - 1}{2} M^2\right) \tag{A.15}$$

$$\frac{p_1}{p_2} = \left(1 + \frac{\gamma - 1}{2} M^2\right)^{\frac{\gamma}{\gamma-1}} \tag{A.16}$$

□

Calculations for equations (3.6)**,** (3.7)**, and** (3.8) **to** (3.9)**.**

Proof:

$$\dot{m}_{ideal} = \rho A V = \frac{p_2}{RT_2} A V = \frac{p_2}{RT_2} A M \sqrt{\gamma R T_2} = \frac{p_2}{\sqrt{RT_2}} A M \sqrt{\gamma} \tag{A.17}$$

$$\dot{m}_{ideal} = \frac{p_1 \left(1 + \frac{\gamma-1}{2} M^2\right)^{-\frac{\gamma}{\gamma-1}}}{\sqrt{RT_1 \left(1 + \frac{\gamma-1}{2} M^2\right)^{-1}}} A M \sqrt{\gamma} \tag{A.18}$$

$$\dot{m}_{ideal} = \frac{p_1}{\sqrt{RT_1}} A M \sqrt{\gamma} \left(1 + \frac{\gamma - 1}{2} M^2\right)^{-\frac{\gamma}{\gamma-1}} \left(1 + \frac{\gamma - 1}{2} M^2\right)^{\frac{1}{2}} \tag{A.19}$$

$$\dot{m}_{ideal} = \frac{p_1}{\sqrt{RT_1}} A M \sqrt{\gamma} \left(1 + \frac{\gamma - 1}{2} M^2\right)^{-\frac{(\gamma+1)}{2(\gamma-1)}} \tag{A.20}$$

□

Calculations for equation (3.9) **to** (3.10)**.**

Proof:

$$\Pi = \left(\frac{p_2}{p_1}\right) \tag{A.21}$$

$$M = \frac{V}{c} = \frac{\sqrt{2c_p(T_1 - T_2)}}{\sqrt{\gamma R T_2}} \tag{A.22}$$

$$M = \sqrt{\left(\frac{2c_p}{\gamma R}\right)\left(\Pi^{-\frac{\gamma-1}{\gamma}} - 1\right)} \tag{A.23}$$

$$M = \sqrt{\left(\frac{2c_p}{\frac{c_p}{c_v}(c_p - c_v)}\right)\left(\Pi^{-\frac{\gamma-1}{\gamma}} - 1\right)} \tag{A.24}$$

$$M = \sqrt{\left(\frac{2}{\gamma - 1}\right)\left(\Pi^{-\frac{\gamma-1}{\gamma}} - 1\right)} \tag{A.25}$$

$$\dot{m}_{ideal} = \frac{p_1}{\sqrt{RT_1}} A\sqrt{\gamma}\sqrt{\left(\frac{2}{\gamma - 1}\right)\left(\Pi^{-\frac{\gamma-1}{\gamma}} - 1\right)}\left(1 + \frac{\gamma - 1}{2}\frac{2}{\gamma - 1}\left(\Pi^{-\frac{\gamma-1}{\gamma}} - 1\right)\right)^{-\frac{(\gamma+1)}{2(\gamma-1)}} \tag{A.26}$$

$$\dot{m}_{ideal} = \frac{p_1}{\sqrt{RT_1}} A\sqrt{\gamma}\sqrt{\left(\frac{2}{\gamma - 1}\right)\left(\Pi^{-\frac{\gamma-1}{\gamma}} - 1\right)}\left(\Pi^{-\frac{\gamma-1}{\gamma}}\right)^{-\frac{(\gamma+1)}{2(\gamma-1)}} \tag{A.27}$$

$$\dot{m}_{ideal} = \frac{p_1}{\sqrt{RT_1}} A\sqrt{\gamma}\sqrt{\left(\frac{2}{\gamma - 1}\right)\left(\Pi^{-\frac{\gamma-1}{\gamma}} - 1\right)}\left(\Pi^{\frac{\gamma+1}{2\gamma}}\right) \tag{A.28}$$

$$\dot{m}_{ideal} = \frac{p_1}{\sqrt{RT_1}} A\sqrt{\left(\frac{2\gamma}{\gamma - 1}\right)\left(\Pi^{-\frac{\gamma-1}{\gamma}} - 1\right)\left(\Pi^{\frac{\gamma+1}{\gamma}}\right)} \tag{A.29}$$

$$\dot{m} = \frac{p_1}{\sqrt{RT_1}} A\sqrt{\frac{2\gamma}{\gamma - 1}\left(\Pi^{\frac{2}{\gamma}} - \Pi^{\frac{\gamma+1}{\gamma}}\right)} \tag{A.30}$$

□

B

Calculations for Non-isentropic Compressible Flow

Proof:

$$\eta_N = \frac{V_{2a}^2}{V_{2s}^2} \tag{B.1}$$

$$\eta_N = \frac{T_1 - T_{2a}}{T_1 - T_{2s}} \tag{B.2}$$

$$\eta_N = \frac{T_1 - T_{2a}}{T_1 - T_1\left(\frac{p_2}{p_1}\right)^{\frac{\gamma-1}{\gamma}}} \tag{B.3}$$

$$\eta_N = \frac{1 - \frac{T_{2a}}{T_1}}{1 - \left(\frac{p_2}{p_1}\right)^{\frac{\gamma-1}{\gamma}}} \tag{B.4}$$

$$\frac{T_{2a}}{T_1} = \underbrace{1 - \eta_N + \eta_N\left(\frac{p_2}{p_1}\right)^{\frac{\gamma-1}{\gamma}}}_{\text{The effective pressure quota } \Pi_{\eta_N}} \tag{B.5}$$

□

Substituting the velocity in equation (3.3) is done the same way as for isentropic flow.

$$\frac{T_1}{T_{2a}} = 1 + \frac{\gamma - 1}{2}M^2 \tag{B.6}$$

Substituting the temperature with velocity in equation (3.18) is done as follows.

Proof:

$$\frac{T_{2a}}{T_1} = 1 - \eta_N\left(1 - \left(\frac{p_2}{p_1}\right)^{\frac{\gamma-1}{\gamma}}\right) \tag{B.7}$$

$$\left(1 + \frac{\gamma-1}{2}M^2\right)^{-1} = 1 - \eta_N\left(1 - \left(\frac{p_2}{p_1}\right)^{\frac{\gamma-1}{\gamma}}\right) \tag{B.8}$$

$$\frac{1}{\eta_N} - \frac{1}{\eta_N\left(1 + \frac{\gamma-1}{2}M^2\right)} = 1 - \left(\frac{p_2}{p_1}\right)^{\frac{\gamma-1}{\gamma}} \tag{B.9}$$

$$1 - \frac{1}{\eta_N} + \frac{1}{\eta_N\left(1 + \frac{\gamma-1}{2}M^2\right)} = \left(\frac{p_2}{p_1}\right)^{\frac{\gamma-1}{\gamma}} \tag{B.10}$$

$$\frac{\eta_N\left(1 + \frac{\gamma-1}{2}M^2\right) - \left(1 + \frac{\gamma-1}{2}M^2\right) + 1}{\eta_N\left(1 + \frac{\gamma-1}{2}M^2\right)} = \left(\frac{p_2}{p_1}\right)^{\frac{\gamma-1}{\gamma}} \tag{B.11}$$

$$\left(\frac{p_1}{p_2}\right)^{\frac{\gamma-1}{\gamma}} = \frac{\eta_N\left(1 + \frac{\gamma-1}{2}M^2\right)}{(\eta_N - 1)\left(1 + \frac{\gamma-1}{2}M^2\right) + 1} \tag{B.12}$$

$$\left(\frac{p_1}{p_2}\right) = \left(\frac{\eta_N\left(1 + \frac{\gamma-1}{2}M^2\right)}{(\eta_N - 1)\left(1 + \frac{\gamma-1}{2}M^2\right) + 1}\right)^{\frac{\gamma}{\gamma-1}} \tag{B.13}$$

$$\left(\frac{p_1}{p_2}\right) = \left(1 + \frac{\gamma-1}{2}M^2\right)^{\frac{\gamma}{\gamma-1}} \underbrace{\left(\frac{\eta_N}{(\eta_N - 1)\left(1 + \frac{\gamma-1}{2}M^2\right) + 1}\right)^{\frac{\gamma}{\gamma-1}}}_{\text{New part of formula with regard to efficiency}} \tag{B.14}$$

□

Furthermore the same approach as for isentropic mass flow is used, however the pressure quota when calculating the Mach number are to be replaced with the effective pressure quota Π_{η_N}.

$$M = \sqrt{\left(\frac{2}{\gamma - 1}\right)\left(\frac{1}{\Pi_{\eta_N}} - 1\right)} \tag{B.15}$$

For simplicity the Mach number in the new term in equation (B.14) is substituted first.

Proof:

$$\left(\frac{\eta_N}{(\eta_N - 1)\left(1 + \frac{\gamma-1}{2}M^2\right) + 1}\right)^{\frac{\gamma}{\gamma-1}} \tag{B.16}$$

$$\left(\frac{\eta_N}{(\eta_N - 1)\left(1 + \frac{\gamma-1}{2}\left(\frac{2}{\gamma-1}\right)\left(\frac{1}{\Pi_{\eta_N}} - 1\right)\right) + 1}\right)^{\frac{\gamma}{\gamma-1}} \tag{B.17}$$

$$\left(\frac{\eta_N}{(\eta_N - 1)\frac{1}{\Pi_{\eta_N}} + 1}\right)^{\frac{\gamma}{\gamma-1}} \tag{B.18}$$

□

The mass flow calculations without the new term is:

Proof:

$$\dot{m}_{part} = \frac{p_1}{\sqrt{RT_1}}A\sqrt{\gamma}\sqrt{\left(\frac{2}{\gamma - 1}\right)\left(\Pi_{\eta_N}^{-1} - 1\right)}\left(1 + \frac{\gamma - 1}{2}\frac{2}{\gamma - 1}\left(\Pi_{\eta_N}^{-1} - 1\right)\right)^{-\frac{(\gamma+1)}{2(\gamma-1)}} \tag{B.19}$$

$$\dot{m}_{part} = \frac{p_1}{\sqrt{RT_1}}A\sqrt{\gamma}\sqrt{\left(\frac{2}{\gamma - 1}\right)\left(\Pi_{\eta_N}^{-1} - 1\right)}\left(\Pi_{\eta_N}^{-1}\right)^{-\frac{(\gamma+1)}{2(\gamma-1)}} \tag{B.20}$$

$$\dot{m}_{part} = \frac{p_1}{\sqrt{RT_1}}A\sqrt{\gamma}\sqrt{\left(\frac{2}{\gamma - 1}\right)\left(\Pi_{\eta_N}^{-1} - 1\right)\left(\Pi_{\eta_N}^{\frac{(\gamma+1)}{(\gamma-1)}}\right)} \tag{B.21}$$

$$\dot{m}_{part} = \frac{p_1}{\sqrt{RT_1}}A\sqrt{\frac{2\gamma}{\gamma - 1}\left(\Pi_{\eta_N}^{\frac{2}{(\gamma-1)}} - \Pi_{\eta_N}^{\frac{(\gamma+1)}{(\gamma-1)}}\right)} \tag{B.22}$$

□

Adding the previous calculated part the full equation for the mass flow with regard to the isentropic efficiency is obtained.

$$\dot{m}_{full} = \frac{p_1}{\sqrt{RT_1}}A\sqrt{\frac{2\gamma}{\gamma - 1}\left(\Pi_{\eta_N}^{\frac{2}{(\gamma-1)}} - \Pi_{\eta_N}^{\frac{(\gamma+1)}{(\gamma-1)}}\right)}\left(\frac{\eta_N}{(\eta_N - 1)(\frac{1}{\Pi_{\eta_N}} + 1)}\right)^{\frac{\gamma}{\gamma-1}} \tag{B.23}$$

C

Calculations for Unsteady Compressible Flow

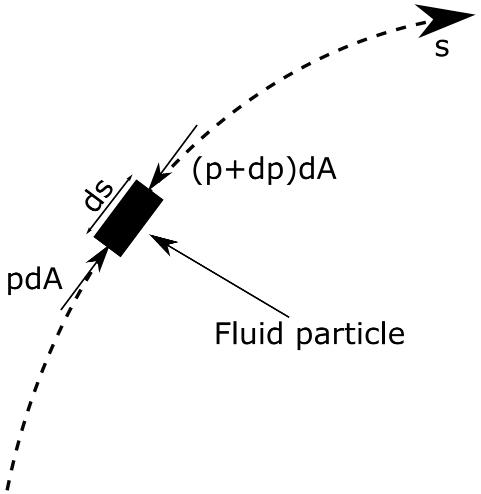

Figure C.1: *An arbitrary fluid particle in an unsteady compressible flow stream, 1-dimension, and no gravity field accounted for.*

Considering the figure C.1 of a fluid particle, with regards to Newton's second law of motion one can do the following simplifications in order to obtain the linear momentum equations.

Proof:

$$\sum F_s = ma_s \tag{C.1}$$

Assuming

$$pdA - (p + dp)dA = m\left(\frac{\partial v ds}{\partial s dt} + \frac{\partial v}{\partial t}\right) \tag{C.2}$$

$$-dpdA = \rho ds dA\left(\frac{\partial v}{\partial s}v + \frac{\partial v}{\partial t}\right) \tag{C.3}$$

$$\frac{1}{\rho}\frac{\partial p}{\partial x} + v\frac{\partial v}{\partial x} + \frac{\partial v}{\partial t} = 0 \tag{C.4}$$

□

Which is how the 1-D linear momentum equation in fluid mechanics is commonly presented. Now substituting the density with the isentropic relation the following calculations can be made.

$$\frac{\rho}{\rho_0} = \left(\frac{p}{p_0}\right)^{\frac{1}{\gamma}} \tag{C.5}$$

$$\frac{1}{\rho_0}\left(\frac{p_0}{p}\right)^{\frac{1}{\gamma}}\frac{\partial p}{\partial x} + v\frac{\partial v}{\partial x} + \frac{\partial v}{\partial t} = 0 \tag{C.6}$$

Furthermore integrating and assuming that $v_0 \approx 0$.

$$\frac{p_0^{\frac{1}{\gamma}}}{\rho_0}\int_{x_0}^{x_t}\frac{1}{p^{\frac{1}{\gamma}}}dp + \frac{v_t^2}{2} + \int_{x_0}^{x_t}\frac{\partial v}{\partial t}dx = 0 \tag{C.7}$$

Replacing the velocity with mass flow.

$$v = \frac{\dot{m}}{\rho A} = \frac{\dot{m}}{\rho_0 A}\left(\frac{p_0}{p}\right)^{\frac{1}{\gamma}} \tag{C.8}$$

$$\frac{p_0^{\frac{1}{\gamma}}}{\rho_0}\int_{x_0}^{x_t}\frac{1}{p^{\frac{1}{\gamma}}}dp + \frac{\dot{m}^2}{2\rho_0^2 A_t^2}\left(\frac{p_0}{p_t}\right)^{\frac{2}{\gamma}} + \frac{p_0^{\frac{1}{\gamma}}}{\rho_0}\int_{x_0}^{x_t}\frac{1}{A}\frac{\partial}{\partial t}\left(\frac{\dot{m}}{p^{\frac{1}{\gamma}}}\right)dx = 0 \tag{C.9}$$

$$\frac{p_0^{\frac{1}{\gamma}}}{\rho_0}\frac{\gamma}{\gamma - 1}\left(p_t^{\frac{\gamma-1}{\gamma}} - p_0^{\frac{\gamma-1}{\gamma}}\right) + \frac{\dot{m}^2}{2\rho_0^2 A_t^2}\left(\frac{p_0}{p_t}\right)^{\frac{2}{\gamma}} + \frac{p_0^{\frac{1}{\gamma}}}{\rho_0}\int_{x_0}^{x_t}\frac{1}{A}\frac{\partial}{\partial t}\left(\frac{\dot{m}}{p^{\frac{1}{\gamma}}}\right)dx = 0 \tag{C.10}$$

Assuming that the dependency of x on $\dot{m}(x)$, and $p(x)$ are negligible in the integral term, the integral can be simplified. Same assumptions is made in (Kiwan et al., 2016) and the result is promising.

$$\frac{p_0^{\frac{1}{\gamma}}}{\rho_0}\frac{\gamma}{\gamma - 1}\left(p_t^{\frac{\gamma-1}{\gamma}} - p_0^{\frac{\gamma-1}{\gamma}}\right) + \frac{\dot{m}^2}{2\rho_0^2 A_t^2}\left(\frac{p_0}{p_t}\right)^{\frac{2}{\gamma}} + \frac{p_0^{\frac{1}{\gamma}}}{\rho_0}\frac{\partial}{\partial t}\left(\frac{\dot{m}}{p_0^{\frac{1}{\gamma}}}\right)\int_{x_0}^{x_t}\frac{dx}{A} = 0 \tag{C.11}$$

Substituting the density with $\rho_0 = \frac{p_0}{T_0 R}$ and and pressure with $\Pi = \frac{p_t}{p_0}$.

$$p_0^{\frac{1}{\gamma}} \frac{\gamma}{\gamma - 1}\left(p_t^{\frac{\gamma-1}{\gamma}} - p_0^{\frac{\gamma-1}{\gamma}}\right) + \frac{\dot{m}^2 T_0 R}{2 p_0 A_t^2}\left(\frac{p_0}{p_t}\right)^{\frac{2}{\gamma}} + p_0^{\frac{1}{\gamma}} \frac{\partial}{\partial t}\left(\frac{\dot{m}}{p_0^{\frac{1}{\gamma}}}\right)\int_{x_0}^{x_t} \frac{dx}{A} = 0 \tag{C.12}$$

$$\frac{\gamma}{\gamma - 1}\left(p_t^{\frac{\gamma-1}{\gamma}} - p_0^{\frac{\gamma-1}{\gamma}}\right) + \frac{\dot{m}^2 T_0 R}{2 A_t^2}\left(\frac{p_0^{\frac{1-\gamma}{\gamma}}}{p_t^{\frac{2}{\gamma}}}\right) + \frac{\partial}{\partial t}\left(\frac{\dot{m}}{p_0^{\frac{1}{\gamma}}}\right)\int_{x_0}^{x_t} \frac{dx}{A} = 0 \tag{C.13}$$

$$p_0^2 \Pi^{\frac{2}{\gamma}} \frac{\gamma}{\gamma - 1}\left(\Pi^{\frac{\gamma-1}{\gamma}} - 1\right) + \frac{\dot{m}^2 T_0 R}{2 A_t^2} + \Pi^{\frac{2}{\gamma}} p_0^{\frac{\gamma+1}{\gamma}} \frac{\partial}{\partial t}\left(\frac{\dot{m}}{p_0^{\frac{1}{\gamma}}}\right)\int_{x_0}^{x_t} \frac{dx}{A} = 0 \tag{C.14}$$

$$\frac{p_0^2 A_t^2}{T_0 R} \frac{2\gamma}{\gamma - 1}\left(\Pi^{\frac{2}{\gamma}} - \Pi^{\frac{\gamma+1}{\gamma}}\right) = \dot{m}^2 + \frac{2 A_t^2}{T_0 R} \Pi^{\frac{2}{\gamma}} p_0^{\frac{\gamma+1}{\gamma}} \frac{\partial}{\partial t}\left(\frac{\dot{m}}{p_0^{\frac{1}{\gamma}}}\right)\int_{x_0}^{x_t} \frac{dx}{A} \tag{C.15}$$

If the last term, containing the dynamics of the flow, in above equation (C.15) is neglected, and A_t is replaced by some area function of the valve opening $A_{eff}(\alpha)$ and C_d is introduced to account for unknown losses the steady compressible orifice equation is acquired.

$$A_{eff} C_d \frac{p_0}{\sqrt{T_0 R}} \sqrt{\frac{2\gamma}{\gamma - 1}\left(\Pi^{\frac{2}{\gamma}} - \Pi^{\frac{\gamma+1}{\gamma}}\right)} = \dot{m} \tag{C.16}$$

Since the geometry in the valve changes depending on the opening angle it is more convenient to replace the integral therm with a dynamic area function, A_{dyn} which have to be determined by dynamic tests. Assuming that the change of p_0 with time is negligible compared to the mass flow change of time, the p_0 term can be extracted from the time derivative. Resulting in the following equation for unsteady, compressible, isentropic, adiabatic, mass flow, similar to the steady compressible equation but with a term for the inertia of the gas.

$$A_{eff}^2 C_d^2 \frac{p_0^2}{T_0 R} \frac{2\gamma}{\gamma - 1}\left(\Pi^{\frac{2}{\gamma}} - \Pi^{\frac{\gamma+1}{\gamma}}\right) = \dot{m}^2 + A_{dyn} A_{eff}^2 C_d^2 \frac{2 p_0}{T_0 R} \Pi^{\frac{2}{\gamma}} \frac{\partial \dot{m}}{\partial t} \tag{C.17}$$

Bibliography

Per Andersson. *Air Charge Estimation in Turbocharged Spark Ignition Engines*. PhD thesis, Linköpings Universitet, December 2005. Cited on pages iii, 2, 3, 6, 9, 11, 12, 20, 27, 31, 41, and 53.

David Chalet, Alexandre Mahe, Jérôme Migaud, and Jean-François Hetet. A frequency modelling of the pressure waves in the inlet manifold of internal combustion engine. *Applied Energy*, 88(9):2988 – 2994, 2011. ISSN 0306-2619. URL `http://www.sciencedirect.com/science/article/pii/S0306261911002066`. Cited on page 7.

Ivan Criscuolo, Oskar Leufven, Andreas Thomasson, and Lars Eriksson. Model-based boost pressure control with system voltage disturbance rejection. In *IFAC World Congress*, Milano, Italy, 2011. Cited on page 11.

Lars Eriksson and Lars Nielsen. *Modeling and Control of Engines and Drivelines*. John Wiley & Sons, 2014. Cited on pages 6, 8, 9, 10, 11, 12, and 27.

Torkel Glad and Lennart Ljung. *Reglerteori : flervariabla och olinjära metoder*. Lund : Studentlitteratur, 2003, 2003. ISBN 9144030037. Cited on page 11.

Torkel Glad and Lennart Ljung. *Reglerteknik : grundläggande teori*. Lund : Studentlitteratur, 2006, 2006. ISBN 9144022751. Cited on page 11.

Elbert Hendricks, Alain Chevalier, Michael Jensen, Spencer C. Sorenson, Dave Trumpy, and Joe Asik. Modelling of the intake manifold filling dynamics. In *SAE Technical Paper*. SAE International, 02 1996. doi: 10.4271/960037. URL `http://dx.doi.org/10.4271/960037`. Cited on pages 2 and 9.

Ingerid Andersson Dan Loyd Karl Storck, Matts Karlsson. *Formelsamling i termo- och fluiddynamik*. Institutionen för ekonomisk och industriell utveckling Tekniska högskolan vid Linköpings universitet, 2012. Cited on pages 5 and 36.

Rani Kiwan, Anna G. Stefanopoulou, Jason Martz, Gopichandra Surnilla, Imtiaz Ali, and Daniel Joseph Styles. Effects of differential pressure measurement characteristics on low pressure-egr estimation error in si-engines*. *IFAC-PapersOnLine*, 49(11):722 – 729, 2016. ISSN 2405-8963. URL `http://www.sciencedirect.com/science/article/pii/S2405896316314550`. 8th {IFAC} Symposium on Advances in Automotive Control {AAC} 2016Norrköping, Sweden, 20—23 June 2016. Cited on pages 8, 22, and 68.

Erik Klasén. Modeling and estimation of long route EGR mass flow in a turbocharged gasoline engine. Master's thesis, Linköping University, SE-581 83 Linköping, 2016. Cited on page 6.

Oskar Leufven and Lars Eriksson. Measurement, analysis and modeling of centrifugal compressor flow for low pressure ratios. *International Journal of Engine Research*, 153(2):153–168, February 2016. Cited on page 11.

Oskar Leufvén and Lars Eriksson. A surge and choke capable compressor flow model—validation and extrapolation capability. *Control Engineering Practice*, 21(12):1871 – 1883, 2013. ISSN 0967-0661. URL `http://www.sciencedirect.com/science/article/pii/S0967066113001354`. Cited on page 11.

Bohan Liang and Robin Holmbom. Boost control with turbo speed sensor and electric wastegate. Master's thesis, Linköping University, SE-581 83 Linköping, 2016. Cited on pages 9 and 11.

James Lighthill. *Waves in fluids*. Cambridge mathematical library. Cambridge : Cambridge Univ. Press, 2001, 2001. ISBN 0521010454. Cited on pages 7 and 8.

Lennart Ljung and Torkel Glad. *Modellbygge och simulering*. Lund : Studentlitteratur, 2004, 2004. ISBN 9144024436. Cited on page 9.

X. Llamas and L. Eriksson. Parameterizing compact and extensible compressor models using orthogonal distance minimization. *Journal of Engineering for Gas Turbines and Power*, 139(1), 2017. ISSN 15288919. Cited on page 11.

V Macián, J M Luján, V Bermúdez, and C Guardiola. Exhaust pressure pulsation observation from turbocharger instantaneous speed measurement. *Measurement Science and Technology*, 15(6):1185, 2004. URL `http://stacks.iop.org/0957-0233/15/i=6/a=020`. Cited on page 8.

Svante Gunnarsson Peter Lindskog Lennart Ljung Johan Löfberg Tomas McKelvey Anders Stenman Martin Enqvist, Torkel Glad and Jan-Erik Strömberg. *IndustriellReglerteknik Kurskompendium*. Bokakademin Linköping, 2014. Cited on page 11.

A. Mehmood, S. Laghrouche, and M. El Bagdouri. Nonlinear modeling of the {VNT} pneumatic actuator with aero-dynamic force. *{IFAC} Proceedings Volumes*, 43(7):518 – 523, 2010. ISSN 1474-6670. URL `http://www.sciencedirect.com/science/article/pii/S1474667015368816`. 6th {IFAC} Symposium on Advances in Automotive Control. Cited on page 10.

H. Ockendon. *Waves and compressible flow*. Texts in applied mathematics: v. 47. New York ; London : Springer, 2003., 2003. ISBN 038740399X. Cited on page 7.

Bernhard Semlitsch, Yue Wang, and Mihai Mihăescu. Flow effects due to pulsation in an internal combustion engine exhaust port. *Energy Conversion and Management*, 86:520 – 536, 2014. ISSN 0196-8904. URL `http://www.sciencedirect.com/science/article/pii/S0196890414005597`. Cited on page 8.

Stephanie Stockar, Marcello Canova, Baitao Xiao, Julia Buckland, and Wen Dai. Modeling for estimation of wave action in multi-cylinder turbocharged {SI} engines. *IFAC-PapersOnLine*, 49(11):708 – 713, 2016. ISSN 2405-8963. URL `http://www.sciencedirect.com/science/article/pii/S2405896316314537`. 8th {IFAC} Symposium on Advances in Automotive Control {AAC} 2016Norrköping, Sweden, 20—23 June 2016. Cited on page 8.

Andreas Thomasson and Lars Eriksson. Effects of pulsating flow on mass flow balance and surge margin in parallel turbocharged engines. In *The 56th Conference on Simulation and Modelling (SIMS 56)*, Linköping, Sweden, 2015. Cited on page 9.

Andreas Thomasson, Oskar Leufvén, Ivan Criscuolo, and Lars Eriksson. Modeling and validation of a boost pressure actuation system, for a series sequentially turbocharged {SI} engine. *Control Engineering Practice*, 21(12):1860 – 1870, 2013. ISSN 0967-0661. URL `http://www.sciencedirect.com/science/article/pii/S0967066113000063`. Cited on page 10.

Zhenyi Yang. Exhaust pressure waves in diesel engines and the impacts on aftertreatment sprays. 2015. Cited on page 7.

Yunus A. Çengel, Robert H. Turner, John M. Cimbala, and Mehmet Kano?lu. *Fundamentals of thermal-fluid sciences*. Singapore : McGraw-Hill, c2012., 2012. ISBN 9780071325110. Cited on pages 6, 8, 13, 16, 18, and 54.